DNA methylation-based reclassification of olfactory neuroblastoma

David Capper[1, 2, 13] *, Nils W. Engel[3, 4] *, Damian Stichel[1] *, Matt Lechner[5, 6, 7], Stefanie Glöss[13], Simone Schmid[13], Christian Kölsche[1, 2], Daniel Schrimpf[1, 2], Judith Niesen[23, 24], Annika K. Wefers[1, 2], David T. W. Jones[8, 9], Martin Sill[8, 9], Oliver Weigert[10], Keith L. Ligon[11], Adriana Olar[12], Arend Koch[13], Martin Forster[6, 7], Sebastian Moran[26], Oscar M. Tirado[27], Miguel Sáinz-Japeado[27], Jaume Mora[28], Manel Esteller[26, 29, 30], Javier Alonso[31], Xavier Garcia del Muro[32], Werner Paulus[14], Jörg Felsberg[15], Guido Reifenberger[15], Markus Glatzel[16], Stephan Frank[17], Camelia M. Monoranu[18], Valerie J. Lund[5, 7], Andreas von Deimling[1, 2], Stefan Pfister[8, 9, 25], Rolf Buslei[19 +], Julika Ribbat-Idel[20 ǂ], Sven Perner[20, ǂ], Volker Gudziol[21], Matthias Meinhardt[22] and Ulrich Schüller[3, 16, 23, 24]

* These authors contributed equally to this work

Correspondence should be addressed to U.S. (u.schueller@uke.de), tel.: +49 (0) 40 7410 – 54968, fax: +49 (0) 40 7410 - 40350

[1] Clinical Cooperation Unit Neuropathology, German Cancer Consortium (DKTK), German Cancer Research Center (DKFZ), Heidelberg, Germany
[2] Department of Neuropathology, University Hospital Heidelberg, Heidelberg, Germany
[3] Center for Neuropathology, Ludwig-Maximilians-University, Munich, Germany
[4] Department of Oncology and Hematology with Sections Bone Marrow Transplant and Pneumology, Hubertus Wald Tumorzentrum / University Cancer Center Hamburg, University Medical Center Hamburg, Hamburg, Germany
[5] Royal National Throat, Nose and Ear Hospital, University College London Hospitals NHS Trust, London, United Kingdom
[6] UCL Cancer Institute, University College London, London, United Kingdom
[7] Head and Neck Centre, University College London Hospitals NHS Trust, London, United Kingdom
[8] Hopp Children's Cancer Center at the NCT Heidelberg (KiTZ), Heidelberg, Germany
[9] Division of Pediatric Neurooncology, German Cancer Consortium (DKTK), German Cancer Research Center (DKFZ), Heidelberg, Germany
[10] Department of Internal Medicine III, University Hospital of the Ludwig-Maximilians-University Munich, Munich, Germany
[11] Department of Medical Oncology and Center for Molecular Oncologic Pathology, Dana-Farber/Brigham and Women's Cancer Center, Harvard Medical School, Boston, MA, USA
[12] Departments of Pathology and Laboratory Medicine and Neurosurgery, Medical University of South Carolina and Hollings Cancer Center, Charleston, SC, USA
[13] Charité – Universitätsmedizin Berlin, corporate member of Freie Universität Berlin, Humboldt-Universität zu Berlin, and Berlin Institute of Health, Institute of Neuropathology, and German Cancer Consortium (DKTK), partner site Berlin, Berlin, Germany
[14] Institute of Neuropathology, University Hospital Münster, Germany
[15] Institute of Neuropathology, Heinrich Heine University, Medical Faculty, Düsseldorf, and German Cancer Consortium (DKTK), partner site Essen/Düsseldorf, Germany
[16] Institute of Neuropathology, University Medical Center Hamburg, Hamburg, Germany
[17] Department of Pathology, Universitätsspital Basel, Basel, Switzerland
[18] Institute of Pathology, Julius-Maximilians-University, Würzburg, Germany
[19] Department of Neuropathology, University of Erlangen, Erlangen, Germany
[20] Institute of Pathology, University Hospital Bonn, Bonn, Germany
[21] ENT Department, Universitätsklinikum Carl Gustav Carus Dresden, Dresden, Germany
[22] Institute for Pathology, Universitätsklinikum Carl Gustav Carus Dresden, Dresden, Germany
[23] Department of Pediatric Hematology and Oncology, University Medical Center, Hamburg-Eppendorf, Germany
[24] Research Institute Children's Cancer Center Hamburg, Hamburg, Germany
[25] Department of Pediatric Oncology, Hematology and Immunology, Heidelberg University Hospital, Heidelberg, Germany
[26] Cancer Epigenetics and Biology Program (PEBC), Bellvitge Biomedical Research Institute (IDIBELL), Barcelona, Catalonia, Spain
[27] Sarcoma Research Group, Molecular Oncology Lab, Bellvitge Biomedical Research Institute (IDIBELL), Barcelona, Catalonia, Spain
[28] Department of Pediatric Onco-Hematology and Developmental Tumor Biology Laboratory, Hospital Sant Joan de Déu, Barcelona, Catalonia, Spain
[29] Department of Physiological Sciences II, School of Medicine, University of Barcelona, Barcelona, Catalonia, Spain,
[30] Institucio Catalana de Recerca i Estudis Avançats (ICREA), Barcelona, Catalonia, Spain
[31] Pediatric Solid Tumor Laboratory, Human Genetic Department, Research Institute of Rare Diseases, Instituto de Salud Carlos III, Madrid, Spain
[32] Oncology Department, ICO-IDIBELL, Barcelona, Spain

+ Current address: Institute of Pathology/Neuropathology, Klinikum am Bruderwald, Sozialstiftung Bamberg, Bamberg, Germany

ǂ Current address: Pathology of the University Hospital Schleswig-Holstein, Campus Lübeck and the Research Center Borstel, Leibniz Center for Medicine and Biosciences, 23538 Lübeck and 23845 Borstel, Germany

Abstract

Olfactory neuroblastoma/esthesioneuroblastoma (ONB) is an uncommon neuroectodermal neoplasm thought to arise from the olfactory epithelium. Little is known about its molecular pathogenesis. For this study, a retrospective cohort of n=66 tumor samples with the institutional diagnosis of ONB was analyzed by immunohistochemistry, genome-wide DNA methylation profiling, copy number analysis, and in a subset, next-generation panel sequencing of 560 tumor-associated genes. DNA methylation profiles were compared to those of relevant differential diagnoses of ONB. Unsupervised hierarchical clustering analysis of DNA methylation data revealed 4 subgroups among institutionally diagnosed ONB. The largest group (n=42, 64%, Core ONB) presented with classical ONB histology and no overlap with other classes upon methylation profiling-based t-distributed stochastic neighbor embedding (t-SNE) analysis. A second DNA methylation group (n=7, 11%) with CpG island methylator phenotype (CIMP) consisted of cases with strong expression of cytokeratin, no or scarce chromogranin A expression and *IDH2* hotspot mutation in all cases. T-SNE analysis clustered these cases together with sinonasal carcinoma with *IDH2* mutation. Four cases (6%) formed a small group characterized by an overall high level of DNA methylation, but without CIMP. The fourth group consisted of 13 cases that had heterogeneous DNA methylation profiles and strong cytokeratin expression in most cases. In t-SNE analysis these cases mostly grouped among sinonasal adenocarcinoma, squamous cell carcinoma and undifferentiated carcinoma.

Copy number analysis indicated highly recurrent chromosomal changes among Core ONB with a high frequency of combined loss of chromosome 1-4, 8-10 and 12. NGS sequencing did not reveal highly recurrent mutations in ONB, with the only recurrently mutated genes being *TP53* and *DNMT3A*.

In conclusion, we demonstrate that institutionally diagnosed ONB are a heterogeneous group of tumors. Expression of cytokeratin, chromogranin A, the mutational status of *IDH2* as well as DNA methylation patterns may greatly aid in the precise classification of ONB.

Introduction

Olfactory neuroblastoma/esthesioneuroblastoma (ONB) is an uncommon neuroectodermal neoplasm of the sinonasal tract and presumed to arise from the olfactory epithelium [7, 14]. Due to its rarity with an estimated incidence of 0.4 per million, accounting of only 2-3 percent of all sinonasal tumors [59], little is known about ONB genetics, molecular biology, or pathogenesis, as tumor tissue samples for comprehensive large-scale studies are limited.

The differential diagnosis of sinonasal “small round blue cell tumors” and tumors with neuroendocrine differentiation at this site is broad and complex [6, 20, 24, 33, 35, 42, 46, 58], including extremely rare entities, such as “Ectopic Sphenoid Sinus Pituitary Adenoma (ESSPA)” [50] and “Non-Small Cell Neuroendocrine Carcinoma of the Sinonasal Tract” [56]. Therefore, misdiagnosis of ONB is likely a common, but underreported problem [10], as histologically defined ONB may include other tumor entities that morphologically mimic ONB. This may in turn impede the reliability of biologic insights drawn from ONB study cohorts and, more importantly, negatively influences treatment decisions and outcomes of patients. A striking historic example

for a misleading study on ONB biology was the report on EWS/FLI1 fusions in four out of six ONB patients [43], which has been subsequently disproven by several other authors [4, 27, 28]. Most likely, these cases represented sinonasal Ewing sarcomas that were classified as ONB due to histological mimicking. A recent study by López-Hernández et al. [29] undertook an assessment of cytokeratin and neuroendocrine immunohistochemical marker expression in a cohort of previously diagnosed ONB, sinonasal neuroendocrine carcinoma and sinonasal undifferentiated carcinoma tumor specimen (n=54 in total) and found more homogenous gene copy number profiles by Affymetrix OncoScan genome-wide copy number profiling for each tumor entity when initial diagnosis was revised by assessment of this narrow set of immunohistochemical markers, indicating better molecular homogeneity of tumor groups after reassessment. The authors proposed correction of diagnosis in 17 of 54 (31 %) of cases whereby ONB seemed to be relatively over-diagnosed initially [29].

Current knowledge on ONB pathobiology mainly derives from comparative genomic hybridization studies of smaller cohorts [5, 19, 29, 41] resulting in the notion of varying complex cytogenetic aberrations and from two independent whole-genome sequencing approaches of individual cases [9, 57].

Three recent studies by *Gay et al.* [18], *Lazo de la Vega et al.* [28] and *Topcagic et al.* [51] independently analyzed larger cohorts of ONB (n=41, n=18 and n=15 cases, respectively) by next-generation sequencing (NGS) methods. They noted heterogeneous, potentially drugable genetic aberrations in up to 51% of tumor samples, but highly recurrent variants were not detected. The *TP53* tumor suppressor gene was mutated in up to 17% of cases in the ONB cohort of *Gay et al.* [19].

The reliability of reported results remains, however, questionable, as the homogeneity of the investigated study cohorts was defined by histology alone, which, in the case of ONB, is rather difficult to distinguish from several differential diagnostic entities.

A recent method to sharpen tumor classification and subsequently diagnostic accuracy is global DNA methylation profiling, which has already led to re-definitions and sub-classifications of various histopathological CNS tumor entities, such as the disintegration of the CNS primitive neuroectodermal tumor (CNS-PNET) entity into several established and four novel tumor entities [44] and sub-classifications of histopathologically defined medulloblastoma [21], ependymal tumors [38], glioblastoma [36, 45], and atypical teratoid/rhabdoid tumors [26]. Moreover, a machine-learning classifier algorithm developed from such a reshaped brain tumor classification offers a proof-of-concept for optimizing diagnostic accuracy in the neuropathological work-up of brain tumors (https://www.molecularneuropathology.org; Capper, Jones, Sill, Hovestadt et al., Nature 2018 in press).

We here analyzed a series of 66 tumors with the institutional diagnosis of ONB using a genome-wide DNA methylation profiling-based approach and secondary integration with histopathological findings. We hereby delineated a purified “Core ONB” group that we then analyzed in more detail concerning molecular traits.

Materials and methods

Patient population

Formalin-fixed, paraffin-embedded (FFPE) tumor samples from 66 patients with the institutional diagnosis of olfactory neuroblastoma (age 9-82) and tumor samples from

n=10 alveolar rhabdomyosarcomas, n=5 pituitary carcinomas, n=6 sinonasal adenocarcinomas, n=2 sinonasal neuroendocrine carcinomas, n=2 *IDH2*-mutant sinonasal carcinomas, n=13 sinonasal squamous−cell carcinomas, and n=8 sinonasal undifferentiated carcinomas (SNUC) were obtained from 9 different medical centers across Germany and from one center each in Switzerland, the United Kingdom, and the USA. Diagnosis was based on the current WHO classification for head and neck tumors [59]. Tissue sample collection, data collection and use were done in accordance with local ethics regulations and approval. Details of the institutional olfactory neuroblastoma cohort are given in Supplementary Table 1.

Additionally, previously published methylation data of n=12 melanomas, n=13 lymphomas, n=23 CNS high grade neuroepithelial tumors with *BCOR* alteration, n=21 CNS high grade neuroepithelial tumors with *MN1* alteration, n=13 Ewing sarcoma family tumors with *CIC* alteration, n=39 CNS neuroblastomas with *FOXR2* activation, n=14 Ewing sarcomas, n=19 paragangliomas, n=95 pituitary adenomas were used for analyses (Capper, Jones, Sill, Hovestadt et al., Nature 2018 in press). The DNA methylation data of single cases from our “Core ONB” samples have been previously published (Capper, Jones, Sill, Hovestadt et al., Nature 2018 in press).

DNA methylation array processing and copy number profiling

DNA was extracted from tumors and analyzed for genome wide DNA methylation patterns using the Illumina HumanMethylation450 BeadChip (450K) array or the Illumina EPIC array. Processing of DNA methylation data was performed with custom approaches as previously described [21, 45]. Copy number profiles were generated using the ‘conumee’ package for “R” environment (http://bioconductor.org/packages/release/bioc/html/conumee.html). Methylation-

class-wide relative copy-number assessment was done based on 450K or EPIC array data by a proprietary algorithm (Stichel, D. and colleagues, unpublished). Euploid levels were determined based on the SNPs included on the BeadChip. The results were controlled by manual inspection of the conumee-based copy number profiles. Clustering was performed using the beta values of the n=25,000 most variably methylated probes as measured by standard deviation. To test for cluster stability, clustering was compared for different numbers of selected most variably methylated probes (range 5,000 to 25,000 probes). Samples were clustered using Pearson correlation coefficient as the distance measure and average linkage (x-axis). Methylation probes were reordered by hierarchical clustering using Euclidean distance and average linkage (y-axis). Additional analysis of tumor subgroups was performed using a t-distributed stochastic neighbor embedding (t-SNE)-based approach [54]. For supplementary t-SNE analysis, available 450K or EPIC array DNA methylation profiles of “small round blue cell” tumor entities and neuroendocrine tumor samples were added (groups equivalent to reference groups of the brain tumor classifier v11b2; detailed information: https://www.molecularneuropathology.org/mnp/classifier/1). For the assessment of relative hyper- or hypomethylation of CpG sites between tumor groups, mean beta-values for single tumor samples were calculated for all CpG-probes of the DNA methylation array to assess “overall CpG methylation” and for CpG probes mapped to CpG islands according to “Relation_to_UCSC_CpG_Island” information from the Infinium MethylationEPIC Array manifest (https://support.illumina.com/array/array_kits/infinium-methylationepic-beadchip-kit/downloads.html) to assess “CpG island methylation”. The distribution of mean-beta values between tumor groups were compared and visualized by box plot diagrams. The distribution of beta-values (“methylation ratio”) of all probes mapped to

CpG islands for individual cases were visually compared between tumor samples using a density estimation plot. For the assessment of CpG island methylator phenotype (CIMP) status, methylation data of brain tumor groups with established CIMP [53] was used for comparison (Astrocytoma, *IDH*-mutant (CIMP), n=77 and Oligodendroglioma, *IDH*-mutant (CIMP), n=60; tumor samples from methylation class reference groups “IDH glioma, subclass 1p/19q codeleted oligodendroglioma” and “IDH glioma, subclass astrocytoma” of the brain tumor classifier v11b2; detailed information: https://www.molecularneuropathology.org/mnp/classifier/1)

Histology and immunohistochemistry (IHC)

FFPE human tumor samples were stained with hematoxylin-eosin (H&E) according to standard protocols. For the assessment of tumor grading of the 66 institutional olfactory neuroblastoma, each sample was independently evaluated by two experienced neuropathologists according to the Hyams grading system of olfactory neuroblastoma [23]. For immunohistochemistry (IHC), the following primary antibodies and concentrations were used: anti-S100: 1:3000 (ab14849, Abcam), anti-chromogranin A: 1:400 (M0869, Dako) and anti-pan-cytokeratin: 1:500 (Z0622, Dako). S100-staining patterns were determined as “nest-surrounding” if >85% of tumor cell nests were encapsulated and demarcated from stroma cells by a closed layer of S100 positive cells. Chromogranin A staining patterns were considered as “homogenous” if >85% of tumor cells showed immunoexpression. Cytokeratin staining was considered “diffuse”, if ≥25% of tumor cells were stained throughout the tissue without local restrictions. All markers were considered “negative”, if <1% of cells were stained. For any staining pattern in-between the mentioned ones, the pattern was labeled as “sparse or focal”, “sparse cells”, or “focal” for the respective marker taking into account the characteristic staining pattern for each marker.

Panel sequencing and targeted *IDH1/2* sequencing

Targeted exon capture and next-generation sequencing of all coding exons of 560 tumor relevant genes (OncoPanel version 3, OPv3) (cf. Supplementary Table 2 for a list of targeted genes) were performed as previously described [3, 55] for a subset of tumor samples (n=20 “Core ONB”, n=3 “Sinonasal tumors with *IDH2* mutation”) with available DNA of sufficient yield and quality. Briefly, concentration of double-stranded DNA was quantified using Quant-iT PicoGreen dsDNA Assay Kit (Life Technologies) and fragmented using Covaris sonication (LE220 Focused-ultrasonicator, Covaris). Fragmented DNA was purified using Agencourt AMPure XP beads (Beckman Coulter, Inc.). Size-selected DNA was then ligated to sequencing adaptors with sample-specific barcodes (KAPA Library Preparation Kit, Roche) and quantified by qPCR. Normalized libraries were pooled and enriched for the exonic regions of the OPv3 genes using the SureSelect Target Enrichment system (Agilent Technologies). The capture pool was sequenced in two lanes of the HiSeq 2500 system (Illumina Inc.) in Rapid Run Mode. Pooled sample reads were de-multiplexed and sorted using the Picard tools (https://broadinstitute.github.io/picard/). Reads were aligned to the reference sequence b37 edition from the Human Genome Reference Consortium using bwa (http://bio-bwa.sourceforge.net/bwa.html) using the following parameters “-q 5 -l 32 -k 2 -o 1” and duplicate reads were identified and removed using the Picard tools. A coverage of ≥30x for >80% of the targets were achieved for all samples.

Mutation analysis for single nucleotide variants (SNVs) and indel calling was performed using Lofreq v2.1.3.1 [60] (http://csb5.github.io/lofreq/). The analysis was run in unpaired mode in the absence of germline probes. Oncotator (http://www.broadinstitute.org/oncotator) was used for annotation. A selection of likely

somatic non-synonymous variants with possible pathogenicity and biologic impact for the respective tumor sample was achieved as follows:

First, variants were filtered using annotation of population frequency from the 6,500 exome release of the Exome Sequencing Project (ESP), and in further consideration of information from dbSNP and COSMIC databases. Variants represented at ≥ 1% in the ESP-European-American population and not listed in COSMIC ≥ 2x were not considered possible pathogenic somatic variants and were removed. Of the remainder, variants listed in dbSNP only and not in COSMIC were also removed. Variants listed both in dbSNP and COSMIC databases were only kept, if available information highlighted a pathogenic variant. Non-synonymy was assumed for variants with Oncotator classification frameshift, initiator codon, missense, nonsense, splice acceptor/donor/region, stop lost or inframe deletion/insertion. All remaining variants were manually reviewed using IGV viewer (http://software.broadinstitute.org/software/igv/).

To predict pathogenic significance of missense SNVs *in silico*, the LR algorithm-based ensemble prediction score from *Dong et al. 2015* [13], which integrates information from nine independent prediction scores and minor allele frequency (MAF) from the 1000 Genomes project [2] was applied and variants labeled as "tolerated" were removed. For the prediction of functional splice site defects, the NNSplice algorithm of *Reese et al. 1997* [39] (http://www.fruitfly.org/seq_tools/splice.html) was used. Frameshift indels were considered pathogenic, with the exception of variants lying at the very 3' end of the gene. Non-frameshift indels were manually reviewed for possible disruption of functionally relevant protein sites.

For the estimation of biological relevance of possibly pathogenic somatic non-synonymous variants, a threshold of ≥ 20% of the sample-specific maximum variant

allele frequency was claimed for assuming a relevant impact on tumor biology. Variants with allele frequency < 20% of sample-specific maximum variant allele frequency were not considered biologically relevant for the individual tumor, but rather assumed to be passenger mutations. The threshold was defined relative to the sample-specific maximum allele frequency under the assumption that the tumor cell content varies between samples and that the maximum sample-specific allele frequency of a variant correlates with the actual tumor cell content of the sample. In cases where the sample-specific maximum variant allele frequency was < 10%, no biologically relevant mutation was assumed.

Pathway assignment and functional categorization of likely pathogenic variants was achieved using DAVID 6.8 (https://david.ncifcrf.gov).

IDH1 and *IDH2* genes were additionally sequenced for all “Sinonasal tumors with *IDH2* mutation” (n=7) and “Sinonasal *IDH2* carcinoma” (n=2) by Sanger sequencing.

Statistical analysis

For the comparison of Hyams grade distributions and distributions of IHC staining patterns for different markers between methylation groups, the Kruskal-Wallis test was applied followed by Dunn’s post test for multiple comparisons between methylation groups. For the comparison of these distributions between “Core ONB A” and “Core ONB B” tumors, the Mann-Whitney test was applied. Baseline characteristics were compared using Kruskal-Wallis and Dunn’s post test for “mean age” and Chi-square test for the comparison of “sex”. The distribution of overall survival (OS) was calculated according to the Kaplan–Meier method. OS was calculated from the date of pathological diagnosis until death of patient from disease or last contact for patients who were still alive. P-values <0.05 were considered

significant. Statistics and graphs were computed with GraphPad Prism 7 (GraphPad Software, Inc.).

Results

Institutionally diagnosed olfactory neuroblastomas are heterogeneous and can be divided into four groups by DNA methylation profiling

Genome-wide DNA methylation profiles of the 66 institutionally diagnosed ONB were generated and analyzed by unsupervised hierarchical clustering (Figure 1). This analysis demonstrated the presence of four clearly demarcated clusters. The formation of clusters was robust for different numbers of CpG probes selected for calculation (data not shown). Of the 66 institutionally diagnosed ONB n=42 (64%) formed the largest group (termed “Core ONB”, Figure 1). Median age for these patients was 62 years (range 20 to 82) and the sex distribution was balanced (Supplementary Figure 4A). In a previous analysis, two subgroups within “Core ONB” were proposed (Capper, Jones, Sill, Hovestadt et al., Nature 2018 in press). We also observed these two subgroups in the here presented larger, partly overlapping data set (Supplementary Figure 1A). However, further analysis indicated that the cluster groups were not robust to perturbation of the number of most variant probes used for cluster analysis with several cases switching between classes. In addition, we were not able to detect histological, immunohistochemical (Supplementary Figure 1B-M), or copy number profile differences (Supplementary Figure 2A, B) between the two groups and thus decided not to separate these two putative ONB sub-clusters for the time being.

A second DNA methylation group consisted of seven cases with a DNA hypermethylation phenotype. This group had both, a strong global but also a strong CpG island methylation (Supplementary Figure 3A-C) reminiscent of the CpG island methylation phenotype (CIMP) observed for *IDH*-mutant gliomas (astrocytomas and oligodendrogliomas) [57]. Indeed, targeted sequencing of *IDH1* and *IDH2* genes revealed R172 *IDH2* hotspot mutations in all cases (see below). The group was therefore provisionally named "Sinonasal tumors with *IDH2* mutation".

A third small cluster group (n=4) among the institutionally diagnosed ONB also had a high level of overall CpG methylation, but in contrast to the "sinonasal tumors with IDH2 mutation" demonstrated no striking CpG island hypermethylation and carried neither IDH1 nor IDH2 mutations (Supplementary Figure 3A-C). This group was provisionally termed “sinonasal tumors, high methylation”, as further defining molecular features could not be identified due to the small number of cases and limited materials. The fourth cluster group consisted of 13 cases with more heterogeneous DNA methylation profiles. This group was provisionally named "Other sinonasal tumors".

T-Distributed Stochastic Neighbor Embedding (t-SNE) analysis of ONB with other methylation classes

To further clarify the origin of the four methylation groups we compared the methylation profiled of the 66 institutionally diagnosed ONB with the methylation profiles of 304 cases of relevant differential diagnoses by t-SNE (Figure 2). In this analysis the "Core ONB" group and the small group "Sinonasal tumors, high methylation" showed no overlap with other classes, further indicating that these likely represent unique tumor classes. In contrast, "Sinonasal tumors with *IDH2* mutation" tightly grouped with the two cases of the recently described group of *IDH2*-mutant

sinonasal carcinoma (“Sinonasal *IDH2* carcinoma”) [12, 25]. The heterogeneous group of 13 "Other sinonasal tumors" did also not form a distinct group but intermixed with cases diagnosed as sinonasal adenocarcinoma, sinonasal squamous cell carcinoma, sinonasal neuroendocrine carcinoma, and sinonasal undifferentiated carcinoma.

Histological reassessment of the four methylation groups constituting institutionally diagnosed ONB

Histological reassessment of “Core ONB” cases demonstrated that these tumors invariably displayed the classical ONB histoarchitecture composed of lobulated tumor cell "nests" demarcated by frequently hyalinized fibrous stroma (Figure 3A). A reminiscent pattern was also seen in the DNA methylation group “Sinonasal tumors, high methylation” (Figure 3C), whereas “Sinonasal tumors with *IDH2* mutation” and “Other sinonasal tumors” exhibited various patterns of histoarchitecture, such as solid growth pattern and comedo-like necrosis (examples in Figure 3B and D). Necrosis was particularly frequent in “Sinonasal tumors with *IDH2* mutation” (6/7 = 87%) and “Other sinonasal tumors”, but not in “Core ONB” cases or “Sinonasal tumors, high methylation”. In line with this, differences were observed concerning the distribution of Hyams grades between the methylation groups with “Core ONB” cases tending to display a low-grade histology with not a single case fulfilling the criteria for a Hyams grade IV (Figure 3Q). In contrast, “Sinonasal tumors with *IDH2* mutation” tended towards high-grade histology.

Immunohistochemistry demonstrated further differences between the methylation groups in line with the results from molecular analyses: the typical pattern of S100 positive sustentacular-like cells surrounding ONB tumor nests was frequently observed in “Core ONB”, “Sinonasal tumors with *IDH2* mutation”, and “Sinonasal

tumors, high methylation", but was never observed in the group of "Other sinonasal tumors" (Figure 3E-H and 3R). Chromogranin A reactivity was also highly enriched in "Core ONB" samples and "Sinonasal tumors, high methylation" but rare in the other two methylation groups (Figure 3I-L, Figure 3S).

According to the current literature, up to one third of ONB cases can exhibit focal staining for cytokeratins [32, 48] and rare cases might even show diffuse reactivity in proportions of tumor tissue [31, 32, 47]. In this cohort, this only held true for a single case within the "Core ONB" group, which displayed diffuse cytokeratin expression (Figure 3T). However, diffuse cytokeratin reactivity was a typical feature of "Sinonasal tumors with *IDH2* mutation" and "Other sinonasal tumors" (Figure 3T; representative staining examples in Figures 3N and P vs. 3M and O).

In this cohort, neither the lack of homogenous chromogranin A immunoreactivity nor diffuse cytokeratin expression excluded the "Core ONB" category, but the combined presence of both features was not seen in any of the "Core ONB" specimens.

From our histological and molecular analyses we conclude, that the methylation group "Core ONB" is closest to the WHO defined entity of ONB [59], and also by DNA methylation signature represents a distinct entity. Tumors of the DNA methylation group "Sinonasal tumors with *IDH2* mutation" show predominant features of undifferentiated high-grade carcinoma and are likely identical to the recently defined "Sinonasal *IDH2* carcinoma" [12, 25]. The DNA methylation group "Other sinonasal tumors" both molecularly and histologically represent an inhomogeneous group likely encompassing various intranasal epithelial tumor entities. Due to the small group size and lack of tissue material, speculation about the underlying histopathological tumor entity of the "Sinonasal tumors, high methylation" group was difficult, but the evaluable samples shared histological similarities to ONB, while differing from sinonasal epithelial tumor entities.

Copy number analysis of “Core ONB” methylation group tumors and “Sinonasal tumors with *IDH2* mutation”

Copy number profiling based on DNA methylation data invariably revealed complex cytogenetic aberrations across all “Core ONB” samples with the predominance of whole chromosomal losses whereas the other 3 methylation groups had less characteristic changes (Figure 4A). Cumulated CNV profiles of the “Core ONB” group revealed a highly recurrent pattern of loss of chromosomes 1, 2, 3, 4, 8, 9, 10, and 12 in almost all cases (Figure 4B). “Sinonasal tumors with *IDH2* mutation” DNA methylation group tumors recurrently harbored combined deletion of chromosomal arm 17p (del(17p)) and gain of 17q (17q+), suggestive of an isochromosome 17q (i(17q) in 5 out of 7 cases (71%) (Figure 4B). The “Sinonasal tumors, high methylation” and “Other sinonasal tumors” groups encompassed a broad spectrum of copy number profiles, ranging from cases with balanced karyotype to cases with highly complex alterations (Figure 4A). Recurrent gene amplifications were not observed within the study cohort. Single amplifications for *CDK6* and *MDM4* (each n=1 sample of “Core ONB”) and *EGFR* (n=1 sample of “Sinonasal tumors with *IDH2* mutation”) were detected.

Mutational spectrum of "Core ONB" and “Sinonasal tumors with *IDH2* mutation”

Genomic profiling by an NGS sequencing approach of a panel of 560 tumor-associated genes (list of covered genes in Supplementary Table 2) was pursued in a subset of 20 “Core ONB” tumors and three “Sinonasal tumors with *IDH2* mutation”. As matched germline was not available, an algorithm for filtering likely somatic non-

synonymous variants and for the assumption of possible pathogenicity and biologic impact was implemented (see materials and methods section). Across all 23 analyzed tumors, n=42 likely somatic and pathologic non-synonymous variants were identified (Supplementary Table 3), including n=32 single-nucleotide polymorphisms (SNPs), n=7 frameshift insertions or deletions (indels) and n=3 splice site defects. Among the “Core ONB”-group (n=20), n=33 variants were detected (Figure 5A). Recurrently mutated genes were *DNMT3A* and *TP53,* both mutated in two cases each (10% of “Core ONB”). The two cases with mutated *TP53* (Sample ID 10 and 13) also harbor a deletion of chromosome 17 in copy number profiling analysis, leading to the assumption of a functionally relevant loss-of-heterozygosity (LOH) in these cases. *TP53* mutations have previously been described in ONB [8, 18, 28, 51, 57]. All other mutated genes were only affected once in our series. A full list of variants of "Core ONB" is given in Figure 5A.

We further analyzed a possible enrichment of the detected "Core ONB" variants in specific signaling pathways or for specific gene function categories (Figure 5B). The most frequently altered signaling pathways were TP53/cell cycle/apoptosis (n=7/20; 35%) and RAS-PIK3-AKT/-MAPK (n=5/20; 25%). Regarding gene function categories, chromatin remodeling (n=5/20; 25%), cell adhesion/migration/cytoskeleton (n=4/20; 20%), transcription regulation (n=3/20; 15%) and DNA repair (n=3/20; 15%) were frequently altered.

Among the three "Sinonasal tumors with *IDH2* mutation" analyzed by panel sequencing the only detected recurrent variants affected the *IDH2* hotspot at codon R172. Targeted sequencing of *IDH1* and *IDH2* revealed further *IDH2* hotspot mutations at codon R172 in all remaining cases of the methylation group *"*Sinonasal tumors with *IDH2* mutation" (n=7 in total). The identified codon R172 alterations comprised four R172S mutations and one R172G, R172T, and R172I mutation. As

known for other types of cancer, the IDH2 mutation is likely causative for the high CpG island methylation level (Supplementary Figure 3B-C) observed in "Sinonasal tumors with *IDH2* mutation" [18]. Two tumor samples of sinonasal carcinomas with known *IDH2* mutations ("Sinonasal *IDH2* carcinoma" in Figure 2) were available for comparison and harbored similar *IDH2* R172 mutations. Given the conformity of "Sinonasal tumors with *IDH2* mutation" from our institutionally diagnosed ONB series and "Sinonasal *IDH2* carcinoma" on the level of methylation profiling, histology and characteristic *IDH2* R172 mutations, identity of these two tumor groups was postulated and led to the uniting definition of "Sinonasal *IDH2* carcinoma". This "Sinonasal *IDH2* carcinoma" designation likely represents a more precise, DNA methylation-based definition of the recently described subset of *IDH2*-mutated SNUCs [12, 25]. Targeted *IDH1* and *IDH2* sequencing in 3 out of 4 samples of "Sinonasal tumors, high methylation" with available material did not reveal an *IDH1* or *IDH2* mutation in this tumor group.

Clinical data assessment

For the DNA methylation groups "Core ONB", "Sinonasal tumors, high methylation", and "Sinonasal *IDH2* carcinoma" the clinical characteristics median age at diagnosis and sex were recorded, and variables were compared between groups by nonparametric testing (Supplementary Figure 4A). The analysis revealed a significantly lower median age at diagnosis for "Sinonasal tumors, high methylation" compared to "Core ONB" tumors and "Sinonasal *IDH2* carcinoma" (28.5y vs. 62y and 52.5y, respectively, p=0.007). In addition, "Sinonasal *IDH2* carcinoma" demonstrated a non-significant imbalance in sex distribution with 7 of 8 manifestations (87.5%) occurring in male patients compared with a balanced sex distribution in "Core ONB" and "Sinonasal tumors, high methylation". Kaplan-Meier analysis for comparison of

overall survival (OS) from time point of diagnosis is shown in Supplementary Figure 4B. However, the limited available retrospective data for DNA methylation groups “Sinonasal tumors, high methylation” and “Sinonasal *IDH2* carcinoma” did not allow for a meaningful calculation of OS and comparative survival assessment.

Discussion

This study describes the molecular dissection of institutionally diagnosed ONB followed by subsequent integration with classical histopathology. This approach led to the identification of four subgroups among cases diagnosed as ONB: a “Core ONB” DNA methylation group with classical ONB histology, mostly representing the traditional concept of ONB according to the WHO classification of head and neck tumors [59]; then a second small group of tumors with a distinct DNA methylation profile and a high level of total DNA methylation, histological features reminiscent of ONB and without *IDH1* or *IDH2* mutations; a third group that both by histology and molecular features could be reclassified as "Sinonasal *IDH2* carcinoma” and a fourth heterogeneous group that showed resemblance to various other sinonasal carcinoma classes by histology and methylation profiling.

These findings indicate that ONB defined by histology alone may be ‘contaminated’ by other tumor entities. Overall, DNA methylation profiling indicates that 36.4% of the tumors of our initial ONB cohort (24 of 66 cases) cannot be considered reliably as ONB, including a substantial subset of cases most likely corresponding to sinonasal carcinomas rather than ONB. This number thus provides an indication of the magnitude of potential ‘contamination’ of histologically defined ONB cohorts by other entities [10, 29].

The “Core ONB” DNA methylation group as the sharply defined representative of the ONB entity is characterized by a classical ONB histology with nest-stroma histoarchitecture, homogenous chromogranin A staining and predominantly absent cytokeratin immunoreactivity. On the contrary, the absence of a homogenous staining pattern for chromogranin A or presence of diffuse cytokeratin immunoreactivity (1/21 and 1/18 in the “Core ONB” group) rendered the diagnosis of tumors of this group highly unlikely and the combination of both features did not occur in any of the “Core ONB” methylation tumors. In contrast to the literature [11, 16, 24, 34, 37, 49], a nest-surrounding S100 staining pattern appeared as an unsuitable criterion for discrimination of ONB from differential diagnoses, as it was also encountered in “Sinonasal tumors, high methylation” and a substantial proportion of “Sinonasal *IDH2* carcinoma”. With respect to grading, “Core ONB” tumors comprise mostly low-grade tumors with Hyams grade IV tumors being absent in this group, questioning the concept of high-grade ONB and therefore the composition of the original cohort used for establishment of the Hyams grading system [23]. Further characterization of “Core ONB” tumors revealed highly recurrent losses of whole chromosome 1, 2, 3, 4, 8, 9, 10, and 12 and showed recurrent mutations of *TP53* and *DNMT3A* (each 10%). *DNMT3A* is a DNA methyltransferase that catalyzes the transfer of a methyl group to the 5′-position of cytosine within a CpG dinucleotide. Mutations of *DNMT3A* (most frequently R882H mutations located in the catalytic domain) are common in AML and are associated with CpG promotor hypomethylation and unfavorable prognosis [17]. One of the two detected *DNMT3A* mutations for ONB in this study can also be localized to the methyltransferase domain of the protein (R688C; tumor sample ID 13). We did not further investigate possible functional consequences of these mutations within this study.

“Sinonasal *IDH2* carcinoma” were characterized by a CpG island methylator phenotype (CIMP) [22], high-grade histology with frequent necrosis, frequent deletions of 17p (likely via isochromosome 17q (i(17q); 71% of cases) and *IDH2* hotspot mutations in 100% of cases [18] as the likely basis of CIMP status [57]. Our histological analysis further demonstrated that they are likely indistinguishable from the recently described *IDH2* mutated SNUCs [12, 25]. DNA hypermethylation of promoter-associated CpG islands of tumor suppressor and DNA repair genes, which leads to transcriptional silencing of these genes, has been recognized as an important epigenetic alteration in human neoplasia [15]. In addition, widespread genome-wide CpG island promoter methylation, also referred to as CIMP, has been described in various tumor types [22] (e.g. colorectal carcinoma [52], neuroblastoma [1], glioblastoma [40] and lower grade glioma [53]) and has been utilized for predicting prognosis and response to treatment [22]. Additionally, our data suggested that “Sinonasal *IDH2* carcinoma” predominantly tend to arise in male patients. Although this finding was not significant, it might reflect a possible effect of lifestyle factors (e.g. tobacco smoke) on pathogenesis of those tumors in contrast to “Core ONB” group tumors or “Sinonasal tumors, high methylation”, which has been emphasized in other head & neck malignancies [40]. Because of the close relation to recently described *IDH2* mutated SNUCs we proposed the name of “Sinonasal *IDH2* carcinoma” for this class of tumors [12, 25]. Our study newly adds CIMP and frequent isochromosome 17q as common molecular features of this class. Concerning the classification, we would consider these cases as separate from other SNUC, as these cases have a highly distinctive methylation pattern different from the remaining SNUC of our series. A similar reordering of tumor classes was previously observed for *IDH*-mutant glioma that are now considered as a separate tumor class from *IDH*-wildtype glioma [30].

The “Sinonasal tumors, high methylation” group remains elusive after this study due to its small size of only four assigned cases and lacking material for insightful histopathologic examination or genomic profiling. However, available histology suggests its similarity to ONB rather than to epithelial tumors. This group characteristically displayed a pronounced level of overall CpG methylation and a preferential manifestation onset in young adult patients. “Sinonasal tumors, high methylation” might represent samples from an unrecognized subgroup of ONB or even a novel rare undefined sinonasal tumor entity.

Our study is in line with various DNA methylation array-based re-definitions and sub-classifications of histopathological CNS tumor entities [21, 26, 36, 38, 45]. The proposed reshaping of the ONB entity herein is another example for the usability and power of array-based genome-wide DNA methylation profiling. Given the vast and complex portfolio of differential diagnoses for sinonasal tumors, a reliable classification of tumors in this location by histology and immunohistochemistry alone might be questionable across various tumor entities, as this study illustrates for ONB, and may imply suboptimal therapy decisions and outcome prediction. In particular, such consideration strongly questions the histopathology-only based diagnostic evaluation in the face of advantageous supplementary methods. The DNA methylation profiling-based brain tumor classifier (https://www.molecularneuropathology.org; Capper, Jones, Sill, Hovestadt et al., Nature 2018 in press) is a proof-of-concept tool for the optimization of diagnostic accuracy for brain tumor differentiation by means of molecular data and the availability of a similar tool for sinonasal tumors would certainly enhance the reliability in sinonasal tumor diagnostics.

Based on our experiences from this study, we have drafted a diagnostic algorithm, intending to strengthen diagnostic accuracy in routine ONB diagnostics starting from

the point of “suspected ONB” based on routine histopathological evaluation (Figure 6). The proposed algorithm may also help for a rational implementation of DNA methylation analysis and *IDH2* sequencing in the routine diagnostic work-up for ONB, which were fundamental for the present study.

Acknowledgements

We are much obliged to the staff of the Center for Cancer Genome Discovery (CCGD) at the Dana-Farber Cancer Institute (Boston, US) for DNA sequencing and especially thank Paul van Hummelen and Aaron Thorner for assistance with interpretation of findings. We thank the Microarray unit of the Genomics and Proteomics Core Facility, German Cancer Research Center (DKFZ) for providing excellent DNA methylation services. We thank the DKFZ-Heidelberg Center for Personalized Oncology (DKFZ-HIPO) for technical support and funding through HIPO_036. In other parts, this work was supported by an Illumina Medical Research Grant. This work was further supported by the Deutsche Krebshilfe and the Fördergemeinschaft Kinderkrebs-Zentrum Hamburg e.V.

Conflict of interest

Andreas von Deimling, David Jones, and David Capper share inventorship of a “DNA-methylation based method for classifying tumor species of the brain“. A patent has been applied for this method (EP 3067432 A1). All terms are being managed by the German Cancer Research Center in accordance with its conflict of interest policies. G. Reifenberger has received research grants from Roche and Merck

Serono, and honoraria for lectures or advisory boards from Amgen and Celldex. The other authors declare no conflicts of interest.

References

1. Abe M, Ohira M, Kaneda A, Yagi Y, Yamamoto S, Kitano Y et al. (2005) CpG Island Methylator Phenotype Is a Strong Determinant of Poor Prognosis in Neuroblastomas. Cancer Res 65: 828-834
2. Abecasis GR, Altshuler D, Auton A, Brooks LD, Durbin RM, Gibbs RA et al. (2010) A map of human genome variation from population-scale sequencing. Nature 467: 1061-1073. Doi: 10.1038/nature09534
3. Abedalthagafi MS, Merrill PH, Bi WL, Jones RT, Listewnik ML, Ramkissoon SH et al. (2014) Angiomatous meningiomas have a distinct genetic profile with multiple chromosomal polysomies including polysomy of chromosome 5. Oncotarget 5: 10596-10606. Doi: 10.18632/oncotarget.2517
4. Argani P, Perez-Ordonez B, Xiao H, Caruana SM, Huvos AG, Ladanyi M (1998) Olfactory neuroblastoma is not related to the Ewing family of tumors: absence of EWS/FLI1 gene fusion and MIC2 expression. Am J Surg Pathol 22: 391-398
5. Bockmuhl U, You X, Pacyna-Gengelbach M, Arps H, Draf W, Petersen I (2004) CGH pattern of esthesioneuroblastoma and their metastases. Brain Pathol 14: 158-163
6. Bridge JA, Bowen JM, Smith RB (2010) The Small Round Blue Cell Tumors of the Sinonasal Area. Head Neck Pathol 4: 84-93. Doi: 10.1007/s12105-009-0158-6

7. Carney ME, O'Reilly RC, Sholevar B, Buiakova OI, Lowry LD, Keane WM et al. (1995) Expression of the human Achaete-scute 1 gene in olfactory neuroblastoma (esthesioneuroblastoma). J Neurooncol 26: 35-43
8. Cha S, Lee J, Shin JY, Kim JY, Sim SH, Keam B et al. (2016) Clinical application of genomic profiling to find druggable targets for adolescent and young adult (AYA) cancer patients with metastasis. BMC Cancer 16: 170. Doi: 10.1186/s12885-016-2209-1
9. Cha S, Lee S-H, Kim J-I, Shin J-Y (2014) Abstract 4191: Whole exome sequencing of a case of olfactory neuroblastoma. Cancer Res 74: 4191. Doi: 10.1158/1538-7445.am2014-4191
10. Cohen ZR, Marmor E, Fuller GN, DeMonte F (2002) Misdiagnosis of olfactory neuroblastoma. Neurosurg focus 12: e3
11. Cordes B, Williams MD, Tirado Y, Bell D, Rosenthal DI, Al-Dhahri SF et al. (2009) Molecular and phenotypic analysis of poorly differentiated sinonasal neoplasms: an integrated approach for early diagnosis and classification. Hum Pathol 40: 283-292. Doi: 10.1016/j.humpath.2008.07.019
12. Dogan S, Chute DJ, Xu B, Ptashkin RN, Chandramohan R, Casanova-Murphy J et al. (2017) Frequent IDH2 R172 mutations in undifferentiated and poorly-differentiated sinonasal carcinomas. J Pathol 242: 400-408. Doi: 10.1002/path.4915
13. Dong C, Wei P, Jian X, Gibbs R, Boerwinkle E, Wang K et al. (2015) Comparison and integration of deleteriousness prediction methods for nonsynonymous SNVs in whole exome sequencing studies. Hum Mol Genet 24: 2125-2137. Doi: 10.1093/hmg/ddu733
14. Engel NW, Neumann JE, Ahlfeld J, Wefers AK, Merk DJ, Ohli J et al. (2016) Canonical Wnt Signaling Drives Tumor-Like Lesions from Sox2-Positive

Precursors of the Murine Olfactory Epithelium. PloS one 11: e0166690. Doi: 10.1371/journal.pone.0166690

15. Esteller M (2008) Epigenetics in Cancer. New England Journal of Medicine 358: 1148-1159. Doi: 10.1056/NEJMra072067

16. Faragalla H, Weinreb I (2009) Olfactory neuroblastoma: a review and update. Adv Anat Pathol 16: 322-331. Doi: 10.1097/PAP.0b013e3181b544cf

17. Ferreira HJ, Heyn H, Vizoso M, Moutinho C, Vidal E, Gomez A et al. (2016) DNMT3A mutations mediate the epigenetic reactivation of the leukemogenic factor MEIS1 in acute myeloid leukemia. Oncogene 35: 3079-3082. Doi: 10.1038/onc.2015.359

18. Gay LM, Kim S, Fedorchak K, Kundranda M, Odia Y, Nangia C et al. (2017) Comprehensive Genomic Profiling of Esthesioneuroblastoma Reveals Additional Treatment Options. The oncologist: Doi: 10.1634/theoncologist.2016-0287

19. Guled M, Myllykangas S, Frierson HF, Jr., Mills SE, Knuutila S, Stelow EB (2008) Array comparative genomic hybridization analysis of olfactory neuroblastoma. Mod Pathol 21: 770-778. Doi: 10.1038/modpathol.2008.57

20. Hafezi S, Seethala RR, Stelow EB, Mills SE, Leong IT, MacDuff E et al. (2011) Ewing's family of tumors of the sinonasal tract and maxillary bone. Head neck pathol 5: 8-16. Doi: 10.1007/s12105-010-0227-x

21. Hovestadt V, Remke M, Kool M, Pietsch T, Northcott PA, Fischer R et al. (2013) Robust molecular subgrouping and copy-number profiling of medulloblastoma from small amounts of archival tumour material using high-density DNA methylation arrays. Acta Neuropathol 125: 913-916. Doi: 10.1007/s00401-013-1126-5

22. Hughes LA, Melotte V, de Schrijver J, de Maat M, Smit VT, Bovee JV et al. (2013) The CpG island methylator phenotype: what's in a name? Cancer Res 73: 5858-5868. Doi: 10.1158/0008-5472.can-12-4306

23. Hyams V (1988) Tumors of the upper respiratory tract and ear. In: Hyams V, Batsakis J, Michaelis L (eds) Atlas of Tumor Pathology. Armed Forces Institute of Pathology, Washington (DC), pp 240-248

24. Iezzoni JC, Mills SE (2005) "Undifferentiated" small round cell tumors of the sinonasal tract: differential diagnosis update. Am J Clin Pathol 124 Suppl: S110-121

25. Jo VY, Chau NG, Hornick JL, Krane JF, Sholl LM (2017) Recurrent IDH2 R172X mutations in sinonasal undifferentiated carcinoma. Mod Pathol 30: 650-659. Doi: 10.1038/modpathol.2016.239

26. Johann PD, Erkek S, Zapatka M, Kerl K, Buchhalter I, Hovestadt V et al. (2016) Atypical Teratoid/Rhabdoid Tumors Are Comprised of Three Epigenetic Subgroups with Distinct Enhancer Landscapes. Cancer Cell 29: 379-393. Doi: 10.1016/j.ccell.2016.02.001

27. Kumar S, Perlman E, Pack S, Davis M, Zhang H, Meltzer P et al. (1999) Absence of EWS/FLI1 fusion in olfactory neuroblastomas indicates these tumors do not belong to the Ewing's sarcoma family. Hum Pathol 30: 1356-1360

28. Lazo de la Vega L, McHugh JB, Cani AK, Kunder K, Walocko FM, Liu CJ et al. (2017) Comprehensive Molecular Profiling of Olfactory Neuroblastoma Identifies Potentially Targetable FGFR3 Amplifications. Mol Cancer Res: Doi: 10.1158/1541-7786.mcr-17-0135

29. Lopez-Hernandez A, Vivanco B, Franchi A, Bloemena E, Cabal VN, Potes S et al. (2018) Genetic profiling of poorly differentiated sinonasal tumours. Sci Rep 8: 3998. Doi: 10.1038/s41598-018-21690-6

30. Louis DN, Perry A, Reifenberger G, von Deimling A, Figarella-Branger D, Cavenee WK et al. (2016) The 2016 World Health Organization Classification of Tumors of the Central Nervous System: a summary. Acta Neuropathol 131: 803-820. Doi: 10.1007/s00401-016-1545-1

31. Meyer C, Hamersley ER, Manosalva RE, Torske K, McIntyre N, Mitchell A (2017) Olfactory Neuroblastoma with Divergent Differentiation: An Unusual Histologic Finding in a Rare Tumor. Head neck Pathol: Doi: 10.1007/s12105-017-0781-6

32. Mills SE (2002) Neuroectodermal neoplasms of the head and neck with emphasis on neuroendocrine carcinomas. Mod Pathol 15: 264-278. Doi: 10.1038/modpathol.3880522

33. Mills SE, Fechner RE (1989) "Undifferentiated" neoplasms of the sinonasal region: differential diagnosis based on clinical, light microscopic, immunohistochemical, and ultrastructural features. Semin Diagn Pathol 6: 316-328

34. Mitchell EH, Diaz A, Yilmaz T, Roberts D, Levine N, DeMonte F et al. (2012) Multimodality treatment for sinonasal neuroendocrine carcinoma. Head & neck 34: 1372-1376. Doi: 10.1002/hed.21940

35. Montone KT (2015) The Differential Diagnosis of Sinonasal/Nasopharyngeal Neuroendocrine/Neuroectodermally Derived Tumors. Arch Pathol Lab Med 139: 1498-1507. Doi: 10.5858/arpa.2014-0383-RA

36. Noushmehr H, Weisenberger DJ, Diefes K, Phillips HS, Pujara K, Berman BP et al. (2010) Identification of a CpG Island Methylator Phenotype that Defines

a Distinct Subgroup of Glioma. Cancer cell 17: 510-522. Doi: 10.1016/j.ccr.2010.03.017

37. Ow TJ, Bell D, Kupferman ME, Demonte F, Hanna EY (2013) Esthesioneuroblastoma. Neurosurg Clin N Am 24: 51-65. Doi: 10.1016/j.nec.2012.08.005

38. Pajtler KW, Witt H, Sill M, Jones DTW, Hovestadt V, Kratochwil F et al. (2015) Molecular Classification of Ependymal Tumors across All CNS Compartments, Histopathological Grades, and Age Groups. Cancer cell 27: 728-743. Doi: 10.1016/j.ccell.2015.04.002

39. Reese MG, Eeckman FH, Kulp D, Haussler D (1997) Improved splice site detection in Genie. Journal of computational biology : a journal of computational molecular cell biology 4: 311-323. Doi: 10.1089/cmb.1997.4.311

40. Rettig EM, D'Souza G (2015) Epidemiology of head and neck cancer. Surg Oncol Clin N Am. 24: 379-396. Doi: 10.1016/j.soc.2015.03.001

41. Riazimand SH, Brieger J, Jacob R, Welkoborsky HJ, Mann WJ (2002) Analysis of cytogenetic aberrations in esthesioneuroblastomas by comparative genomic hybridization. Cancer Genet Cytogenet 136: 53-57

42. Soldatova L, Campbell RG, Carrau RL, Prevedello DM, Wakely P, Jr., Otto BA et al. (2016) Sinonasal Carcinomas with Neuroendocrine Features: Histopathological Differentiation and Treatment Outcomes. J Neurol Surg Part B, Skull base 77: 456-465. Doi: 10.1055/s-0036-1582432

43. Sorensen PH, Wu JK, Berean KW, Lim JF, Donn W, Frierson HF et al. (1996) Olfactory neuroblastoma is a peripheral primitive neuroectodermal tumor related to Ewing sarcoma. Proc Natl Acad Sci U S A 93: 1038-1043

44. Sturm D, Orr BA, Toprak UH, Hovestadt V, Jones DTW, Capper D et al. (2016) New Brain Tumor Entities Emerge from Molecular Classification of CNS-PNETs. Cell 164: 1060-1072. Doi: 10.1016/j.cell.2016.01.015

45. Sturm D, Witt H, Hovestadt V, Khuong-Quang DA, Jones DT, Konermann C et al. (2012) Hotspot mutations in H3F3A and IDH1 define distinct epigenetic and biological subgroups of glioblastoma. Cancer Cell 22: 425-437. Doi: 10.1016/j.ccr.2012.08.024

46. Su SY, Bell D, Hanna EY (2014) Esthesioneuroblastoma, neuroendocrine carcinoma, and sinonasal undifferentiated carcinoma: differentiation in diagnosis and treatment. Int Arch Otorhinolaryngol 18: S149-156. Doi: 10.1055/s-0034-1390014

47. Sugita Y, Kusano K, Tokunaga O, Mineta T, Abe M, Harada H et al. (2006) Olfactory neuroepithelioma: an immunohistochemical and ultrastructural study. Neuropathology 26: 400-408

48. Taxy JB, Bharani NK, Mills SE, Frierson HF, Jr., Gould VE (1986) The spectrum of olfactory neural tumors. A light-microscopic immunohistochemical and ultrastructural analysis. Am J Surg Pathol 10: 687-695

49. Thompson LD (2009) Olfactory neuroblastoma. Head Neck Pathol 3: 252-259. Doi: 10.1007/s12105-009-0125-2

50. Thompson LDR, Seethala RR, Müller S (2012) Ectopic Sphenoid Sinus Pituitary Adenoma (ESSPA) with Normal Anterior Pituitary Gland: A Clinicopathologic and Immunophenotypic Study of 32 Cases with a Comprehensive Review of the English Literature. Head Neck Pathol 6: 75-100. Doi: 10.1007/s12105-012-0336-9

51. Topcagic J, Feldman R, Ghazalpour A, Swensen J, Gatalica Z, Vranic S (2018) Comprehensive molecular profiling of advanced/metastatic olfactory

neuroblastomas. PLoS One 13: e0191244. Doi: 10.1371/journal.pone.0191244

52. Toyota M, Ahuja N, Ohe-Toyota M, Herman JG, Baylin SB, Issa J-PJ (1999) CpG island methylator phenotype in colorectal cancer. Proceedings of the National Academy of Sciences 96: 8681-8686. Doi: 10.1073/pnas.96.15.8681

53. Turcan S, Rohle D, Goenka A, Walsh LA, Fang F, Yilmaz E et al. (2012) IDH1 mutation is sufficient to establish the glioma hypermethylator phenotype. Nature 483: 479-483. Doi: 10.1038/nature10866

54. van der Maaten L, Hinton G (2008) Visualizing high-dimensional data using t-SNE. J Mach Learn Res 9: 2579–2605

55. Wagle N, Berger MF, Davis MJ, Blumenstiel B, Defelice M, Pochanard P et al. (2012) High-throughput detection of actionable genomic alterations in clinical tumor samples by targeted, massively parallel sequencing. Cancer Discov 2: 82-93. Doi: 10.1158/2159-8290.CD-11-0184

56. Weinreb I, Perez-Ordoñez B (2007) Non-Small Cell Neuroendocrine Carcinoma of the Sinonasal Tract and Nasopharynx. Report of 2 Cases and Review of the Literature. Head and Neck Pathol 1: 21-26. Doi: 10.1007/s12105-007-0004-7

57. Weiss GJ, Liang WS, Izatt T, Arora S, Cherni I, Raju RN et al. (2012) Paired tumor and normal whole genome sequencing of metastatic olfactory neuroblastoma. PloS one 7: e37029. Doi: 10.1371/journal.pone.0037029

58. Wenig BM (2009) Undifferentiated malignant neoplasms of the sinonasal tract. Arch Pathol Lab Med 133: 699-712. Doi: 10.1043/1543-2165-133.5.699

59. Wenig BM, Dulguerov P, Kapadia SB, Prasad ML, Fanburg-Smith JC, Thompson LDR (2005) Chapter 1: Tumours of the Nasal Cavity and Paranasal Sinuses. Neuroectodermal tumors. Olfactory nueroblastoma. In: Barnes L,

Eveson J, Reichart P, Sidransky D (eds) Pathology & Genetics of Head and Neck Tumours, 3rd Edition, Volume 9. IARCPress, Lyon, pp 66-70.

60. Wilm A, Aw PP, Bertrand D, Yeo GH, Ong SH, Wong CH et al. (2012) LoFreq: a sequence-quality aware, ultra-sensitive variant caller for uncovering cell-population heterogeneity from high-throughput sequencing datasets. Nucleic Acids Res 40: 11189-11201. Doi: 10.1093/nar/gks918

Figure legends

Figure 1. DNA methylation profiling-based cluster analysis of institutionally diagnosed olfactory neuroblastoma (ONB). Unsupervised hierarchical cluster analysis of DNA methylation profiles from n=66 tumor samples with the institutional diagnosis of olfactory neuroblastoma, using the 25,000 most variant probes, resulted in 3 clusters and an additional group of tumors with heterogeneous DNA methylation profiles (“Other sinonasal tumors”, n=13). The largest group consisted of n=42 cases and was designated as "Core ONB”. The cluster “Sinonasal tumors, high methylation” (n=4) showed a pronounced overall CpG methylation. “Sinonasal tumors with *IDH2* mutation” (n=7) displayed a CpG island methylator phenotype (CIMP).

Figure 2. t-SNE analysis of institutionally diagnosed ONB combined with differential diagnoses. t-distributed Stochastic Neighbor Embedding (t-SNE) analysis of DNA methylation profiles from tumor samples included in the cluster analysis (n=66) (annotated & color coded according to “Methylation group” color code in Figure 1) supported the stratification into 4 DNA methylation groups: an ONB core group (“Core ONB”, n=42) and 3 additional groups: “Sinonasal tumors, high methylation” (n=4), “Sinonasal tumors with *IDH2* mutation” (n=7) and “Other

sinonasal tumors" (n=13). Inclusion of methylation profiling data from differential diagnoses of ONB (n=304 samples; tumor group annotations within and below right-hand corner of the figure) revealed no overlap between "Core ONB" and "Sinonasal tumors, high meth." with any other tumor group, supporting the uniqueness of these tumor classes. "Sinonsal tumors with *IDH2* mutations" converged with Sinonasal *IDH2* carcinoma, suggesting identity of these tumor groups. "Other sinonasal tumors" intermixed with samples from several tumor groups, in particular with various sinonasal carcinoma entities and likely represent misdiagnosed sinonasal carcinomas.

Figure 3. Histological reassessment of institutionally diagnosed ONB in relation to DNA methylation grouping. The DNA methylation groups "Core ONB", "Sinonasal tumors with *IDH2* mutation", "Sinonasal tumors, high methylation" and "Other sinonasal tumors" were histologically reassessed (H&E staining; A-D) and analyzed for immunohistochemical expression patterns of S100 (E-H), chromogranin A (I-L) and cytokeratin (M-P). Images (A-P) illustrate representative staining results for each marker in each group. Arrow in B indicates area of necrosis in a representative "Sinonasal tumor with *IDH2* mutation" case. Scale bar is 100 µm (only visualized in A). Bar graphs in Q-T display comparisons of distributions of values for variables "Hyams grade" (Q), "S100" (R), "chromogranin A" (S) and "cytokeratin" (T) between tumor groups. Staining patterns for each marker have been operationalized by categorization (categories shown beneath "Key"). Distributions for each variable were compared between tumor groups via Kruskal-Wallis and Dunn's post testing for multiple comparisons. The "Sinonasal tumors, high methylation" group was excluded from this analysis, due to low case numbers. Brackets indicate group comparisons with significantly different distribution of values for a certain variable.

Figure 4. Overview of copy number variation (CNV) profiles and comparison of CNV profiles between "Core ONB"- & "Sinonasal tumors with *IDH2* mutation"-groups. A, CNV profiles of all n=66 tumor samples with the institutional diagnosis of ONB in the same clustering order as in Figure 1. "Core ONB" (n=42) group tumors showed prominent cytogenetic aberrations with highly recurrent losses of several chromosomes while "Sinonasal tumors, high methylation" (n=4) and "Sinonasal tumors with *IDH2* mutation" (n=8) revealed less total cytogenetic aberrations. B. Representative copy number profiles of example cases of group "Core ONB" and "Sinonasal tumors with *IDH2* mutation" are depicted in the upper half. Gains represent positive (color coded green), losses negative (color coded red) deviations from the baseline for chromosomes 1-22, x and y. Integration of single CNV profiles of all methylation group members led to cumulated CNV profiles of the respective tumor groups (lower half of panel B). The rate of gains/losses across the group is indicated at the y-axis.

Figure 5. Mutations in "Core ONB" group tumors. A. Tabular overview of detected variants in n=20 "Core ONB" samples analyzed by panel sequencing of 560 tumor-associated genes. Reported variants were likely non-synonymous somatic mutations filtered for possible pathogenicity and biological impact. Sample IDs correspond to the order of samples from the initial cluster analysis (Figure 1) from left to right (see S1 and S3 Table). 14 of 20 (70%) of "Core ONB" samples were found to harbor mutations in at least one gene. dbNSFP-Ensemble-LR-Prediction-Score results for *in silico* prediction of pathogenicity were reported for SNVs. A value of ≥0.5 represents "damaging". Depicted variants scoring below 0.5 were kept in this overview due to other evidence on possible pathogenicity. B. Overview of recurrently

altered signaling pathways & gene functions. All genes mutated for a certain pathway or gene functional category across all "Core ONB" samples are listed on the right.

Figure 6. An algorithm for improvement of diagnostic accuracy in ONB diagnostics. The proposed algorithm starts from the point of "suspected ONB" after standard histopathological work-up. Depending on the specific characteristics of an individual case, up to three diagnostic steps are suggested. After initial assessment of chromogranin A and cytokeratin staining and Hyams grading, the diagnosis ONB can be rejected or accepted with high reliability for a proportion of cases. For Hyams high-grade tumors, we suggest *IDH2* sequencing to allow for the diagnosis of "Sinonasal IDH2 carcinoma" in mutated cases. We recommend DNA methylation analysis with DNA methylation array processing and subsequent brain tumor classifier analysis (https://www.molecularneuropathology.org) for Hyams high-grade tumors without *IDH2* mutations and Hyams low-grade tumors with either non-homogenous chromogranin A or diffuse cytokeratin staining results. For tumor samples matching towards the two aforementioned categories, diagnosis of either ONB, "Sinonasal tumor with high methylation" or "Other sinonasal tumor" (which presumably includes various sinonasal tumor differential diagnoses) is possible and final assignment benefits from DNA methylation profiling. Values for sensitivity, specificity and negative predictive value (NPV) were calculated for selected paths from application of this algorithm to the original institutionally diagnosed ONB cohort (n=66) of this study.

Supplementary Figure 1. Analysis of possible sub-clusters within "Core ONB". A. Unsupervised hierarchical cluster analysis of DNA methylation data from "Core

ONB" group samples (n=42) of the initial methylation cluster analysis revealed further subdivision of the "Core ONB" DNA methylation group into two putative clusters: "Core ONB A" (n=24) and "Core ONB B" (n=18). B. The methylation subgroups "Core ONB A" and "Core ONB B" were compared on the level of histomorphology (H&E staining; B-C) and for expression patterns of selected immunohistochemical markers S100 (E-F), chromogranin A (H-I) and cytokeratin (K-L). The images illustrate representative staining results for each marker in both groups. Scale bar is 100 µm (only visualized in B). Bar graphs display comparisons of distributions of values for variables "Hyams grade" (D) as well as "S100" (G), "chromogranin A" (J) and "cytokeratin" (M) between tumor groups. The distributions of staining patterns between "Core ONB A" and "Core ONB B" tumors did not differ significantly for any variable tested (D, G, J and M).

Supplementary Figure 2. Comparative copy number variation (CNV) profiling of DNA methylation subgroups "Core ONB A" and "Core ONB B". A. CNV profiles of the n=42 "Core ONB" tumor samples are displayed according to the clustering order of Supplementary Figure 1 with highlighted subdivision into putative methylation subgroups "Core ONB A" (n=24) and "Core ONB B" (n=18). B. The comparison of cumulated CNV profiles between "Core ONB A" and "Core ONB B" showed identical complex cytogenetic aberrations with recurrent losses of chromosomes 1, 2, 3, 4, 8, 9, 10, and 12 in both groups, further justifying their merge to an "Core ONB" DNA methylation group.

Supplementary Figure 3. Assessment of overall CpG methylation and CpG island methylation levels. A. The distribution of mean beta-values for all CpG-probes of the methylation array was displayed as box-plots for the sinonasal tumor

groups “Core ONB”, Sinonasal *IDH2* carcinoma”, “Sinonasal tumors, high meth.”, Other sinonasal tumors” and two additional brain tumor groups with established CIMP status (*IDH*-mutated astrocytoma and oligodendroglioma) to allow for comparison of “overall CpG methylation” between tumor groups. “Sinonasal *IDH2* carcinoma” and “Sinonasal tumors, high meth.” demonstrated relatively high overall CpG methylation. B. The same analysis for CpG probes of the methylation array mapped to CpG islands revealed similar high levels of CpG island methylation between CIMP reference brain tumor groups and “Sinonasal *IDH2* carcinoma”, prompting the assumption of CIMP status for this group in accordance with detected recurrent *IDH2* mutations. C. Density plot analysis of the distribution of beta-values (“methylation ratio”) of all probes mapped to CpG islands for individual tumor samples confirmed relative hypermethylation of CpG islands for tumor samples of the “Sinonasal *IDH2* carcinoma” methylation group in comparison to “Core ONB” and “Other sinonasal tumors”. An individual case from the “Sinonasal tumors, high methylation” group showed similar pronounced CpG island methylation, but no *IDH1/2*-mutation.

Supplementary Figure 4. Baseline characteristics and survival analysis of tumor groups. A. Baseline characteristics of tumor groups: The clinical attributes “Median age” and “Sex” were operationalized and compared by Kruskal-Wallis and Dunn’s post testing for “Median age” and by Chi-square testing for “Sex” between tumor groups. “Median age” was significantly different between “Core ONB” and “Sinonasal tumors, high methylation”. B. Kaplan-Meier survival analysis for tumor groups: A meaningful calculation of overall survival (OS) and group comparison was not possible due to limited clinical follow-up data.

Supplementary Table 1. Overview of the institutionally diagnosed (histopathologically defined) olfactory neuroblastoma cohort.

(attached excel file)

Supplementary Table 2. List of genes included in the OncoPanel version 3 exome sequencing panel.

(attached excel file)

Supplementary Table 3. List of likely somatic non-synonymous variants with possible pathogenic and biological impact in "Core ONB" and "Sinonasal tumors with *IDH2* mutation".

(attached excel file)

Figure 1

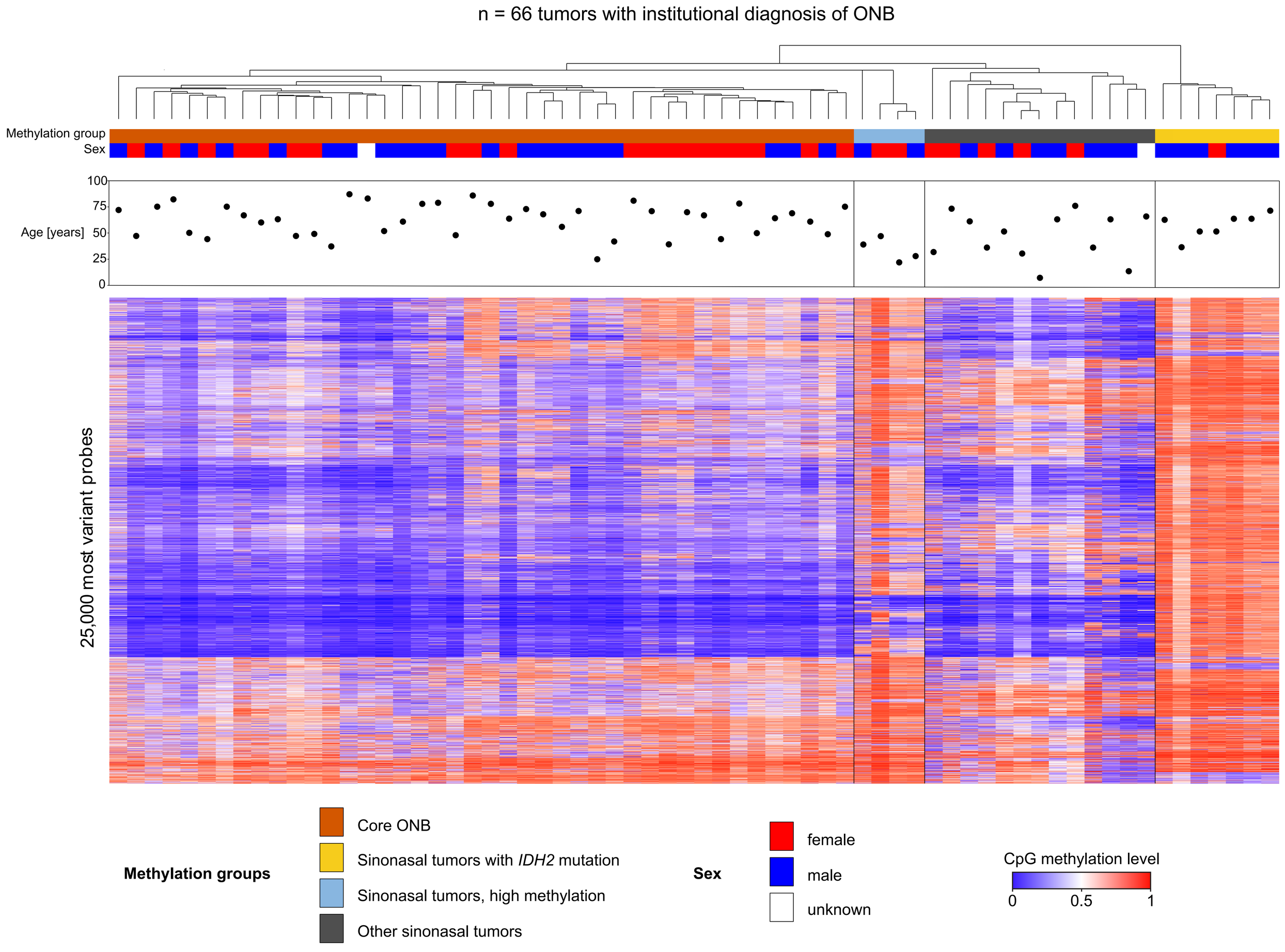

Figure 2

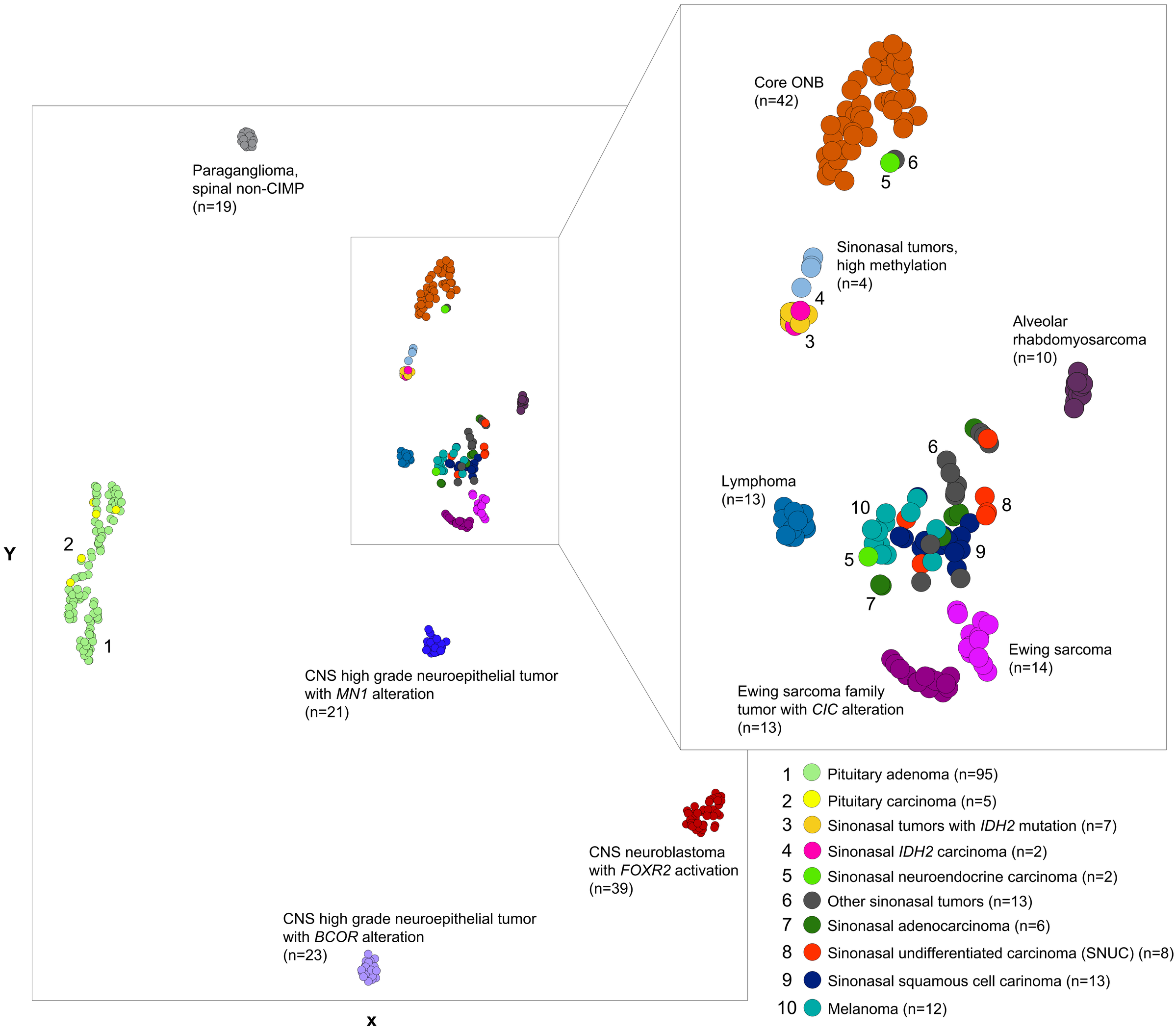
Paraganglioma,
spinal non-CIMP
(n=19)
2
1
Y
CNS high grade neuroepithelial tumor
with *MN1* alteration
(n=21)
CNS high grade neuroepithelial tumor
with *BCOR* alteration
(n=23)
CNS neuroblastoma
with *FOXR2* activation
(n=39)
x
Core ONB
(n=42)
6
5
Sinonasal tumors,
high methylation
(n=4)
4
3
Alveolar
rhabdomyosarcoma
(n=10)
Lymphoma
(n=13)
6
10
8
5
9
7
Ewing sarcoma
(n=14)
Ewing sarcoma family
tumor with *CIC* alteration
(n=13)
1 Pituitary adenoma (n=95)
2 Pituitary carcinoma (n=5)
3 Sinonasal tumors with *IDH2* mutation (n=7)
4 Sinonasal *IDH2* carcinoma (n=2)
5 Sinonasal neuroendocrine carcinoma (n=2)
6 Other sinonasal tumors (n=13)
7 Sinonasal adenocarcinoma (n=6)
8 Sinonasal undifferentiated carcinoma (SNUC) (n=8)
9 Sinonasal squamous cell carinoma (n=13)
10 Melanoma (n=12)

Figure 3

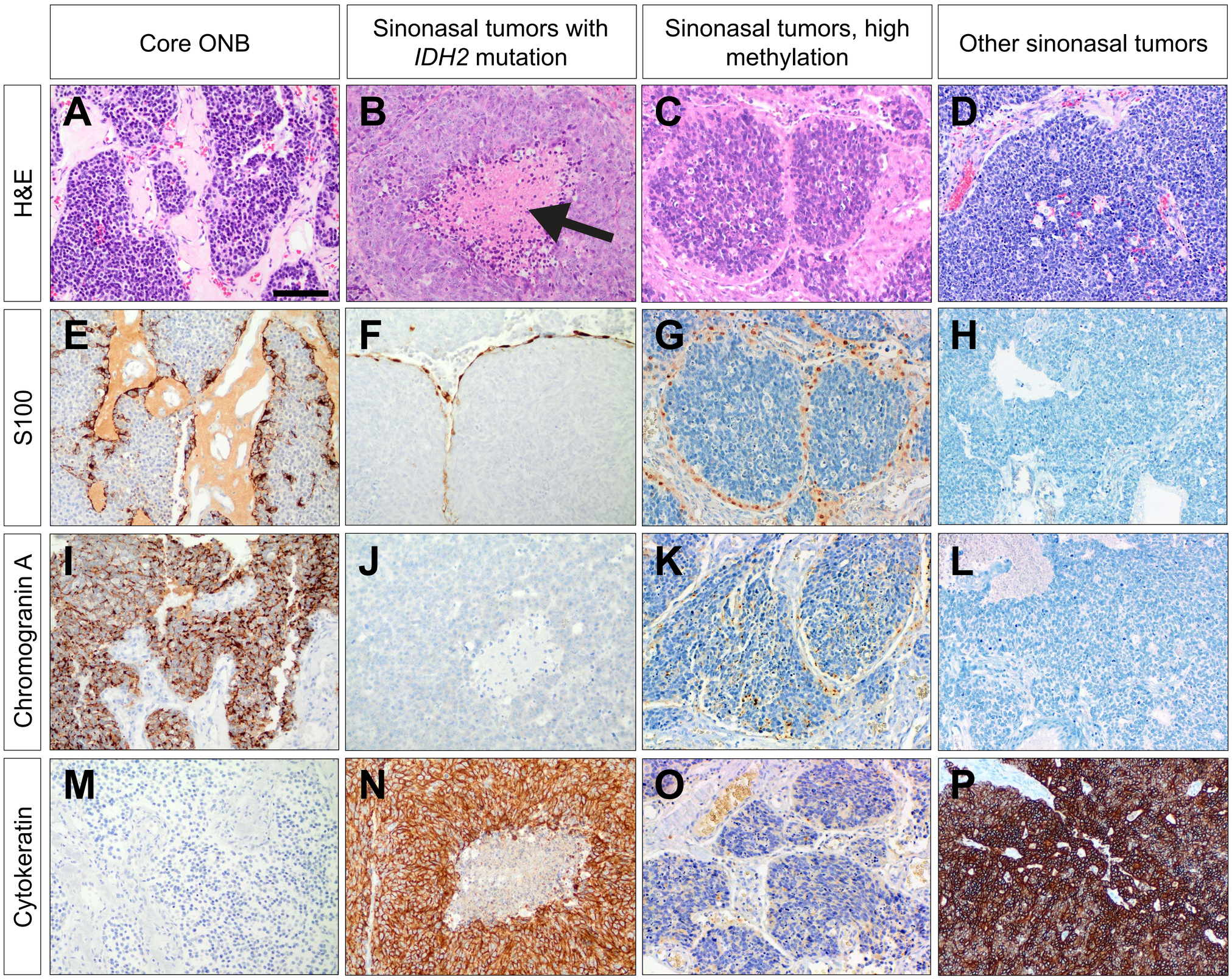

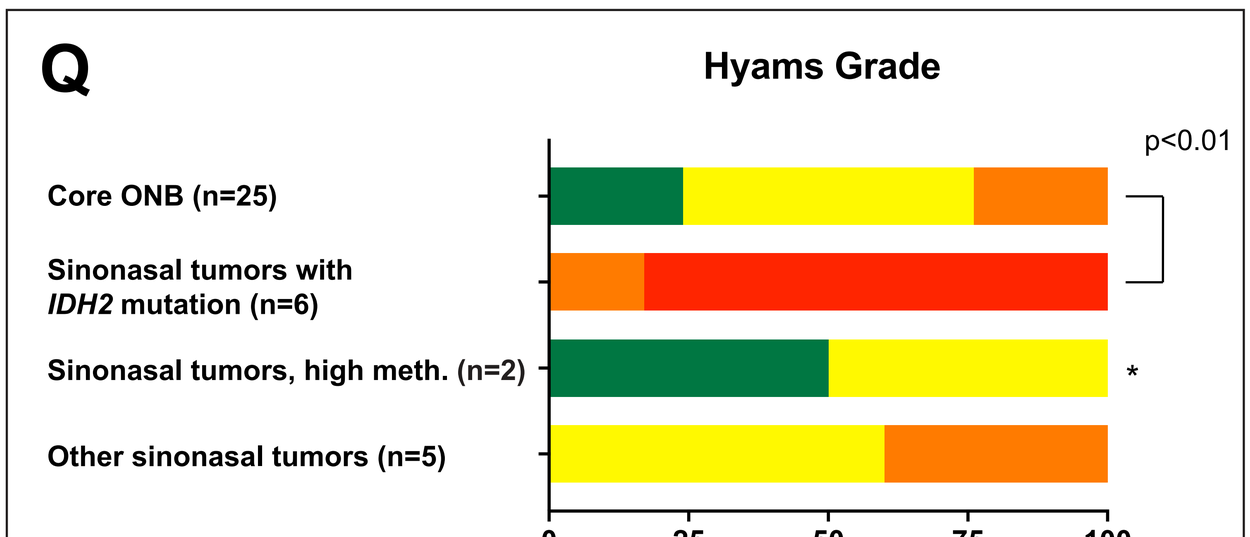

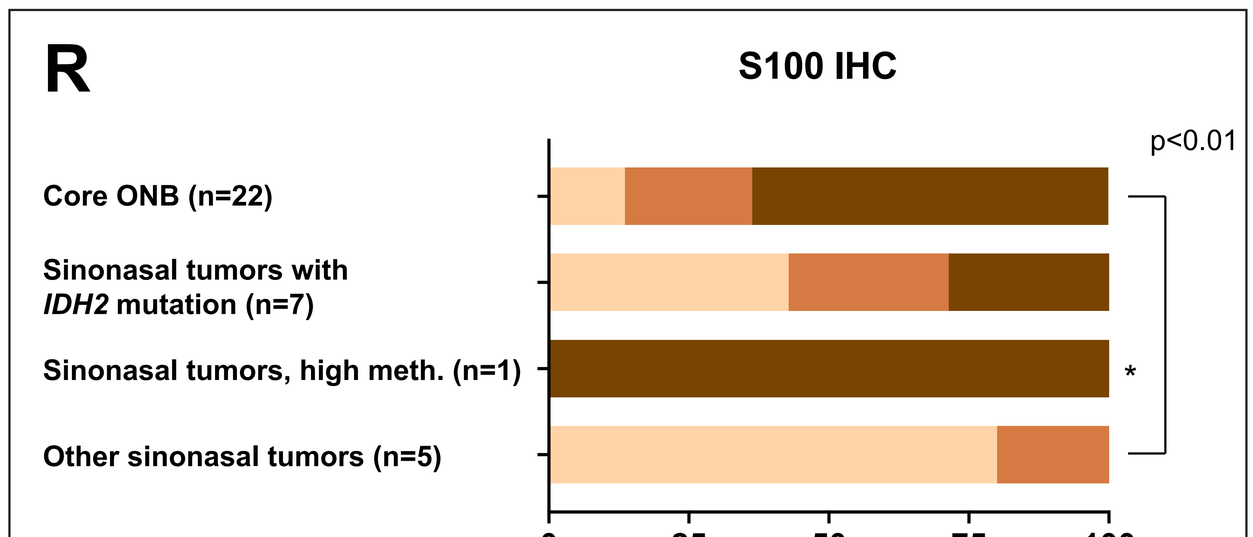

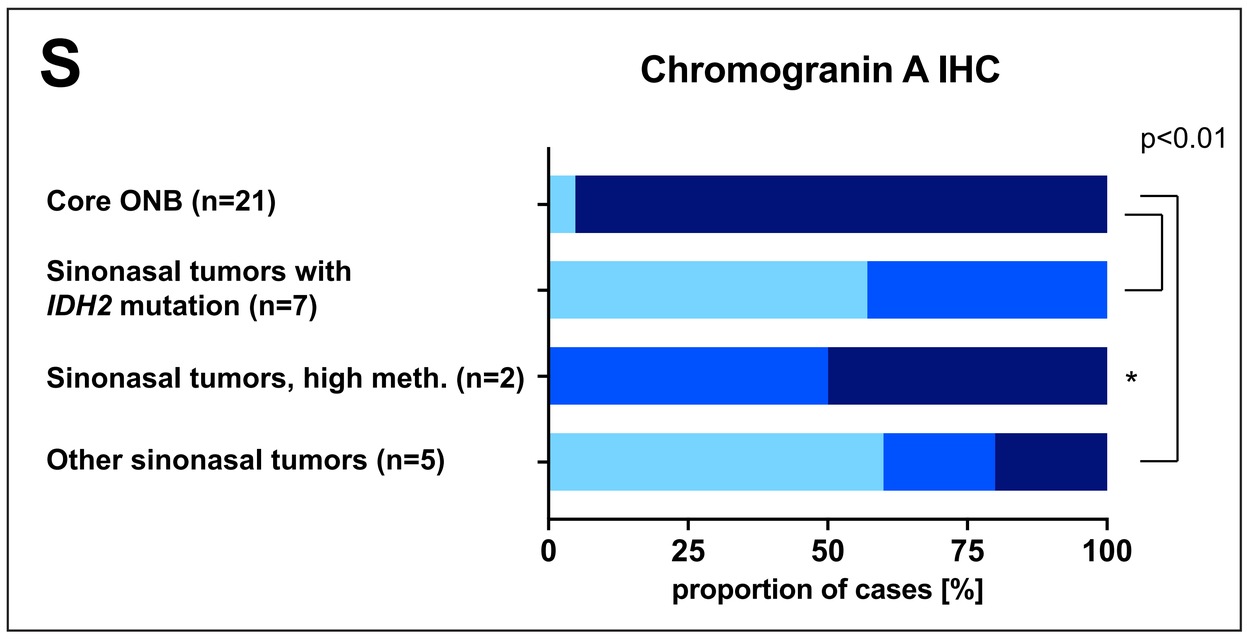

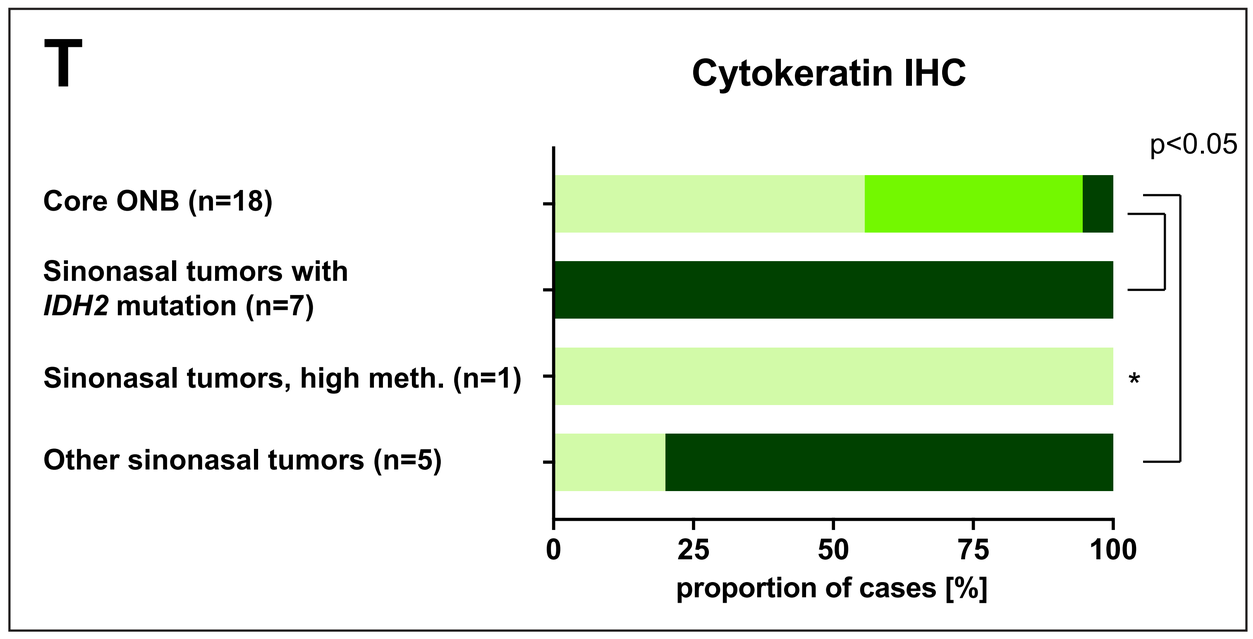

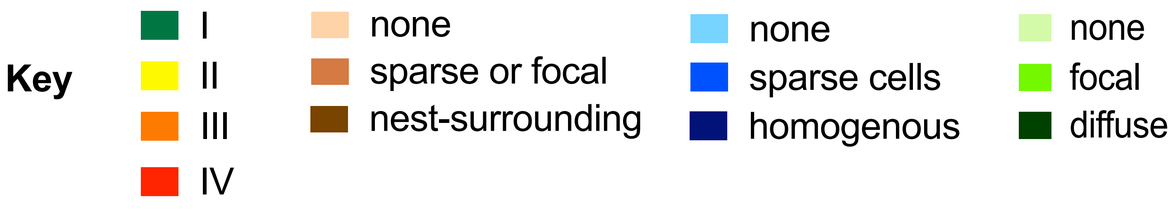

*Sinonasal tumors, high meth. excluded for statistical analysis as too few samples were available for analysis

Figure 4

A

n = 66 tumors with institutional diagnosis of ONB

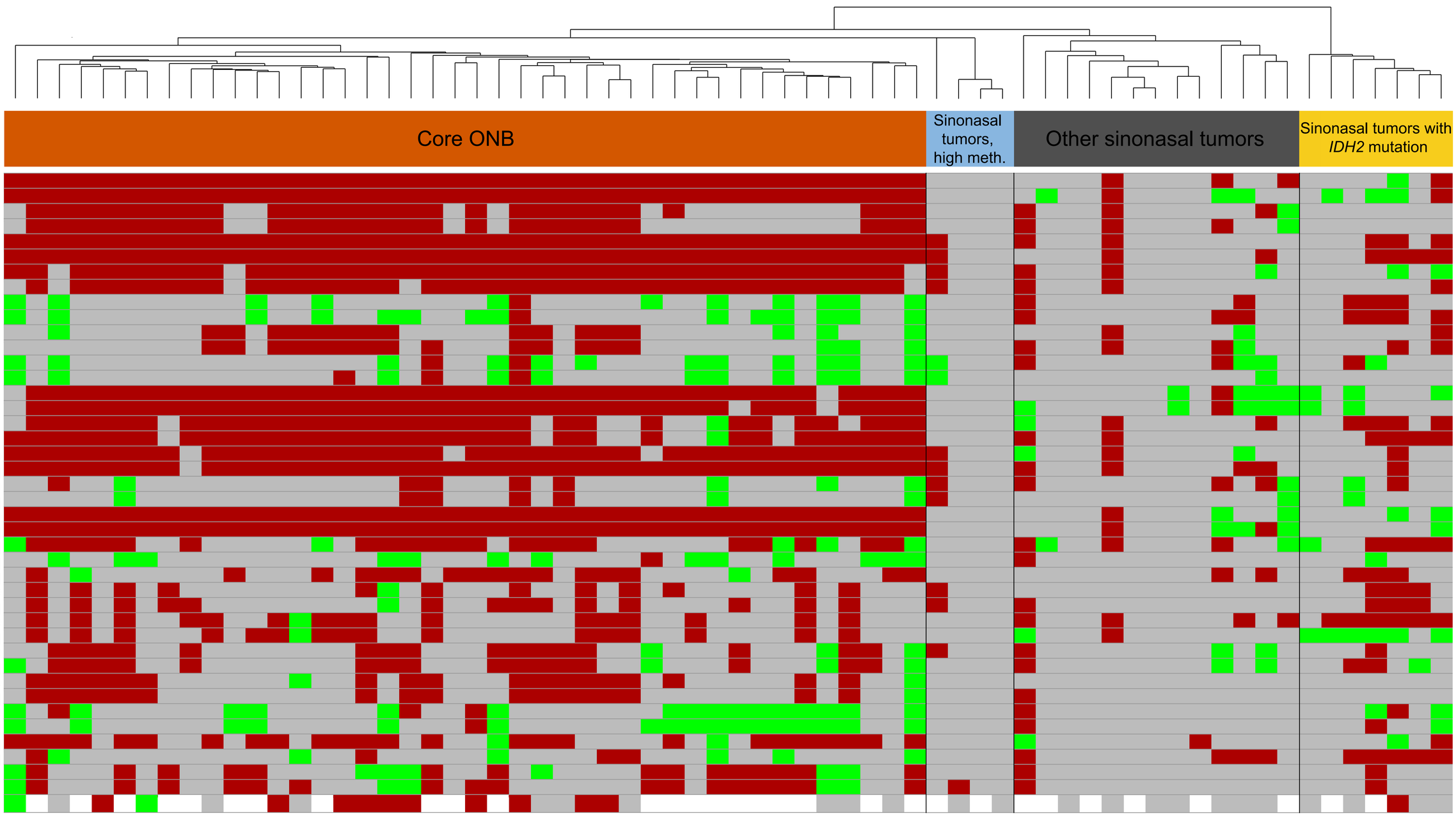

Copy number variations (CNVs) gain balanced loss not defined

B

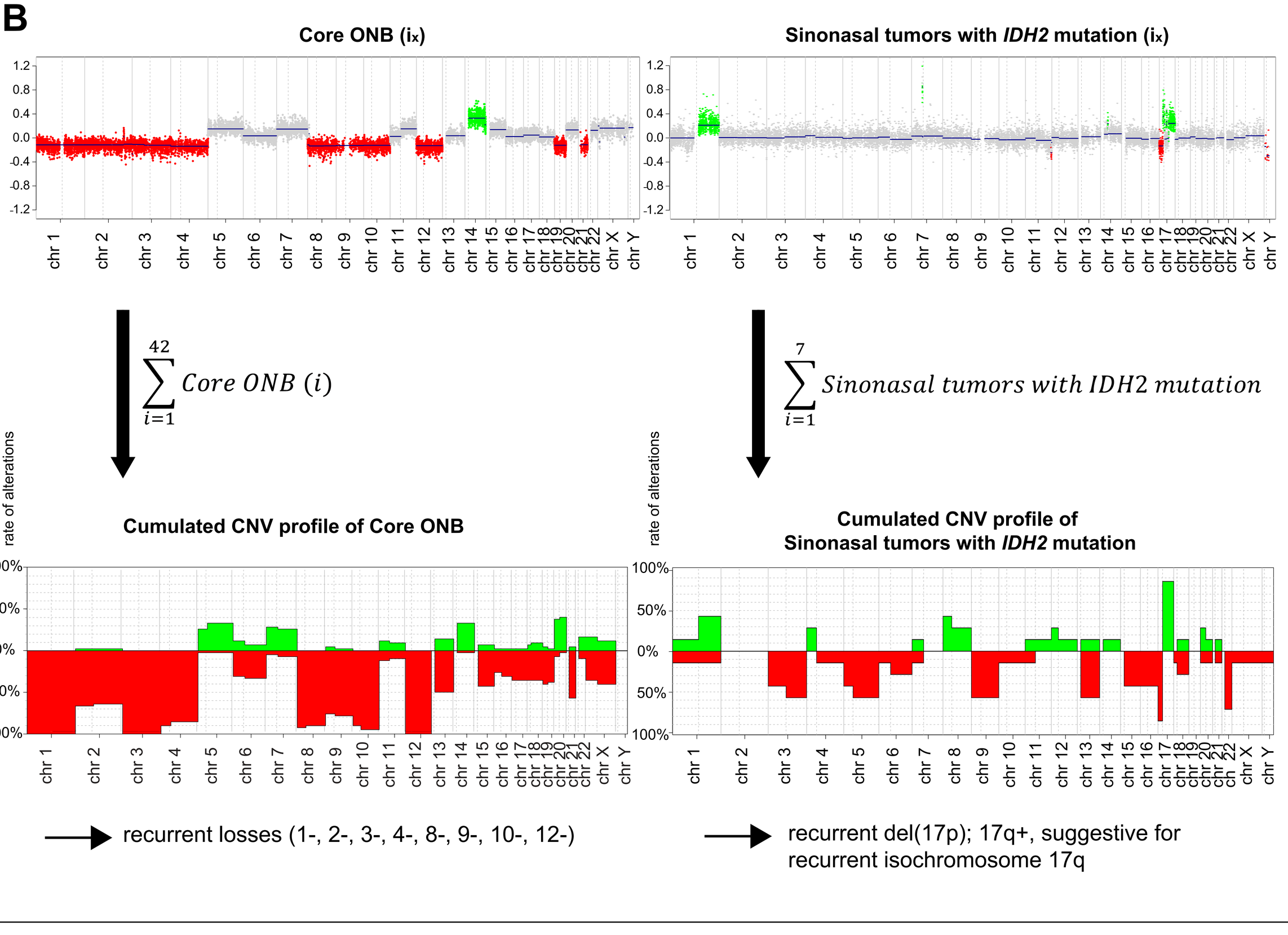

Figure 5

A

Sample ID	Gene	Type of variant	cDNA-Change	Protein-Change	dbNSFP-Ensemble-LR-Prediction-Score	Allele Frequency
5	*JAK3*	Missense	c.2164G>A	p.V722I	0.085	0.096
6	*LRP2*	Missense	c.764G>T	p.G255V	0.923	0.760
10	*EP300*	Missense	c.4195G>C	p.D1399H	0.990	0.217
10	*TP53*	Missense	c.1031T>G	p.L344R	0.897	0.297
13	*ATRX*	Frameshift Deletion	c.1185_1186delTA	p.FK395fs		0.780
13	*DNMT3A*	Missense	c.2062C>T	p.R688C	0.505	0.181
13	*INSR*	Missense	c.2276G>A	p.R759Q	0.604	0.407
13	*KMT2D*	Missense	c.8101C>T	p.R2701W	0.697	0.644
13	*MET*	Missense	c.3029C>T	p.T1010I	0.376	0.465
13	*MET*	Missense	c.2329A>G	p.T777A	0.569	0.439
13	*MSH6*	Frameshift Deletion	c.1128_1133delAAAGAG	p.KR377del		0.713
13	*MYH11*	Missense	c.1097A>G	p.N366S	0.641	0.377
13	*SMARCA4*	Missense	c.4777G>A	p.V1593I	0.763	0.333
13	*TP53*	Missense	c.524G>A	p.R175H	0.996	0.770
14	*CRBBP*	Missense	c.3718T>G	p.C1240G	0.925	0.335
15	*GNAS*	Missense	c.10C>T	p.R4C	0.588	0.464
15	*TP73*	Missense	c.1670C>T	p.A557V	0.880	0.234
24	*ABL1*	Missense	c.868A>G	p.M290V	0.770	0.295
27	*MAP3K9*	Missense	c.2881C>G	p.L961V	0.590	0.487
30	*CDH2*	Splice Site				0.135
30	*KMT2C*	Frameshift Deletion	c.5065_5066delGA	p.E1689fs		0.115
30	*SOX10*	Missense	c.1284G>T	p.M428I	0.555	0.432
30	*ZMYM2*	Splice Site				0.203
32	*DNMT3A*	Missense	c.1313A>C	p.D438A	0.727	0.488
32	*FLT4*	Missense	c.1459C>G	p.R487G	0.634	0.479
32	*PIK3C2B*	Missense	c.2698C>T	p.R900C	0.669	0.143
32	*PKHD1*	Missense	c.4895G>A	p.G1632D	0.539	0.496
32	*SP3*	Missense	c.1934A>T	p.H645L	0.580	0.355
36	*MSH2*	Missense	c.662G>C	p.G221A	0.813	0.864
38	*XPC*	Missense	c.940C>T	p.R314W	0.560	0.352
39	*CDKN2C*	Frameshift Insertion	c.413_414insAC	p.D138fs		0.111
39	*SLC22A2*	Missense	c.1309T>G	p.C437G	0.584	0.520
40	*SETBP1*	Missense	c.2627A>G	p.N876S	0.772	0.917

B

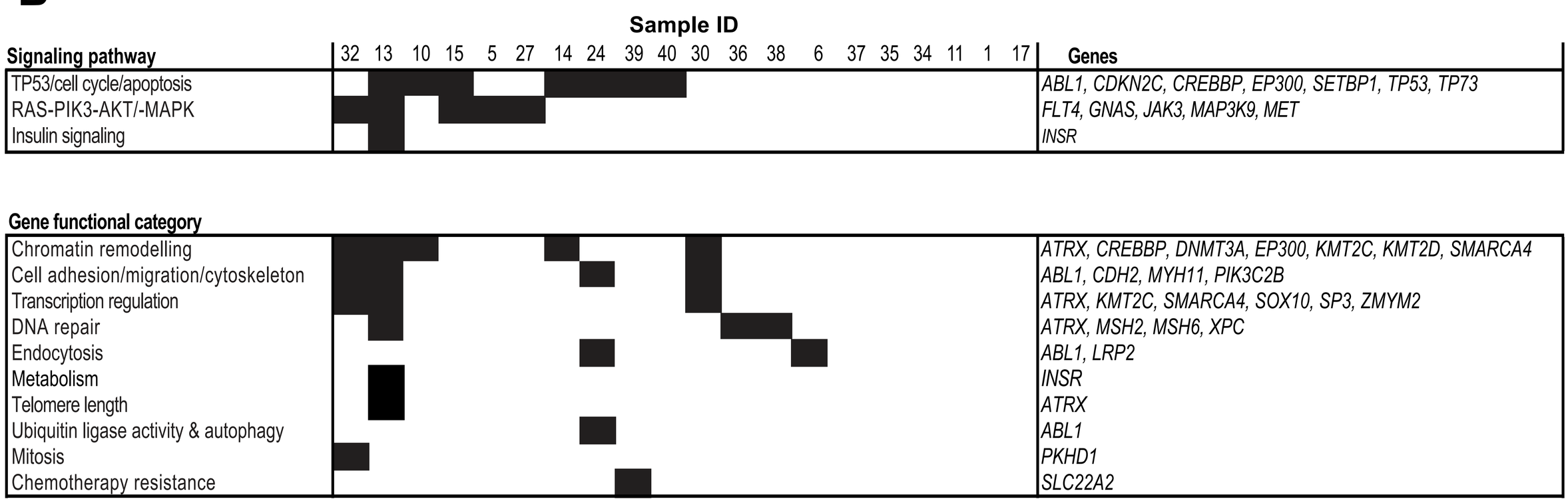

Figure 6

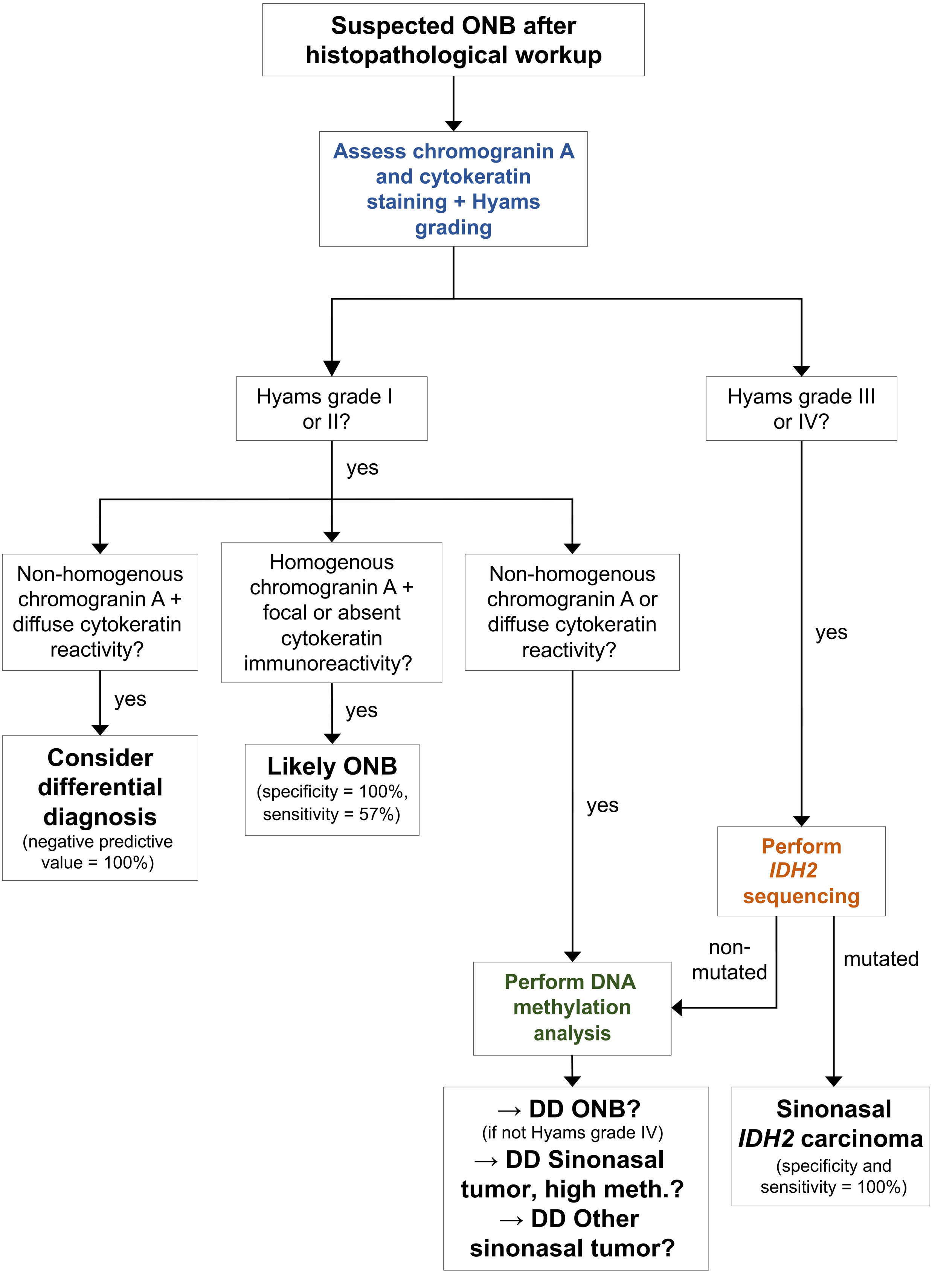
Suspected ONB after histopathological workup
Assess chromogranin A and cytokeratin staining + Hyams grading
Hyams grade I or II?
Hyams grade III or IV?
yes
Non-homogenous chromogranin A + diffuse cytokeratin reactivity?
Homogenous chromogranin A + focal or absent cytokeratin immunoreactivity?
Non-homogenous chromogranin A or diffuse cytokeratin reactivity?
yes
yes
yes
yes
Consider differential diagnosis
(negative predictive value = 100%)
Likely ONB
(specificity = 100%, sensitivity = 57%)
Perform IDH2 sequencing
non-mutated
mutated
Perform DNA methylation analysis
→ DD ONB?
(if not Hyams grade IV)
→ DD Sinonasal tumor, high meth.?
→ DD Other sinonasal tumor?
Sinonasal IDH2 carcinoma
(specificity and sensitivity = 100%)

Supplementary Figure 1

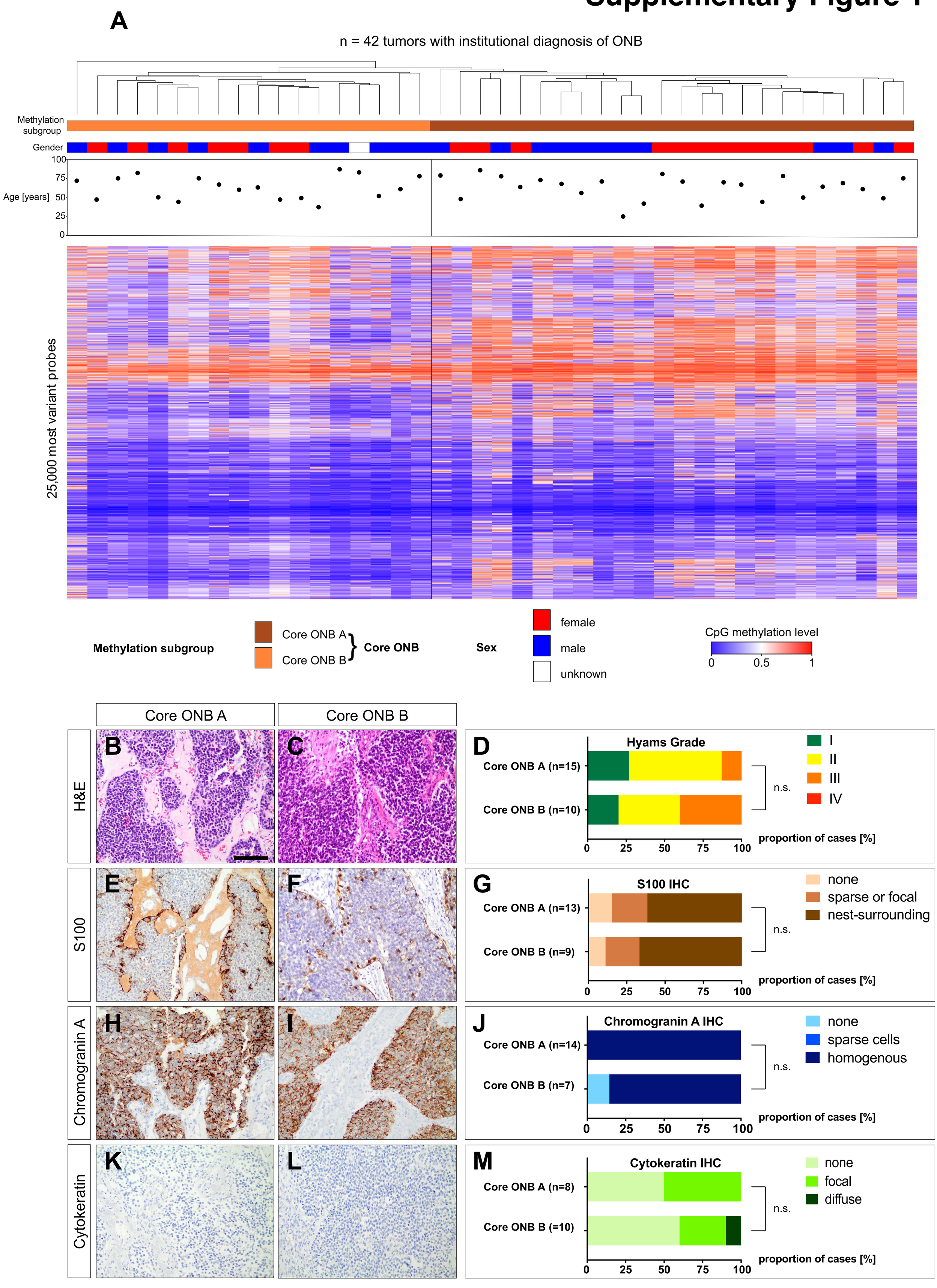

Supplementary Figure 2

A

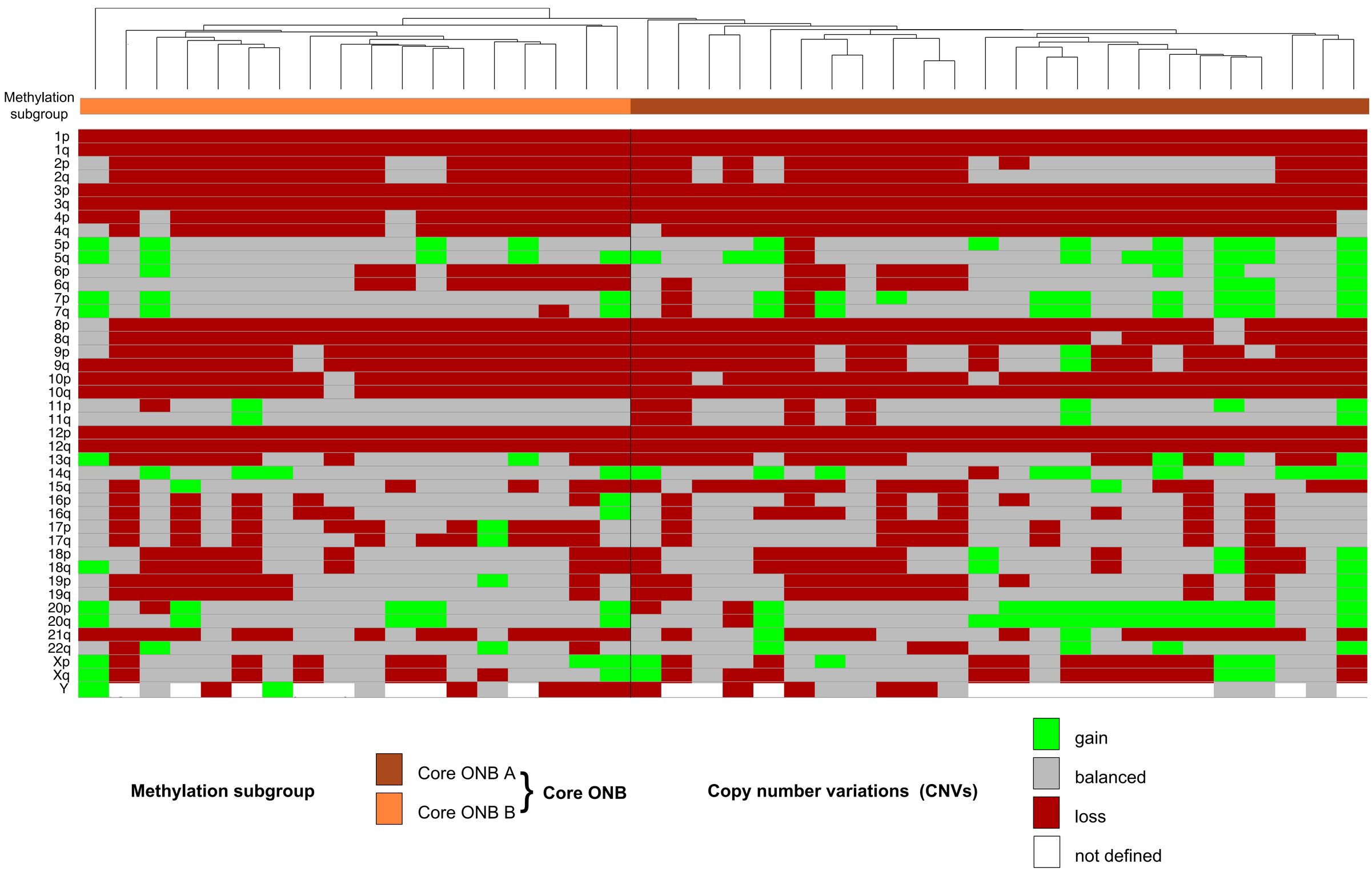

B

Supplementary Figure 3

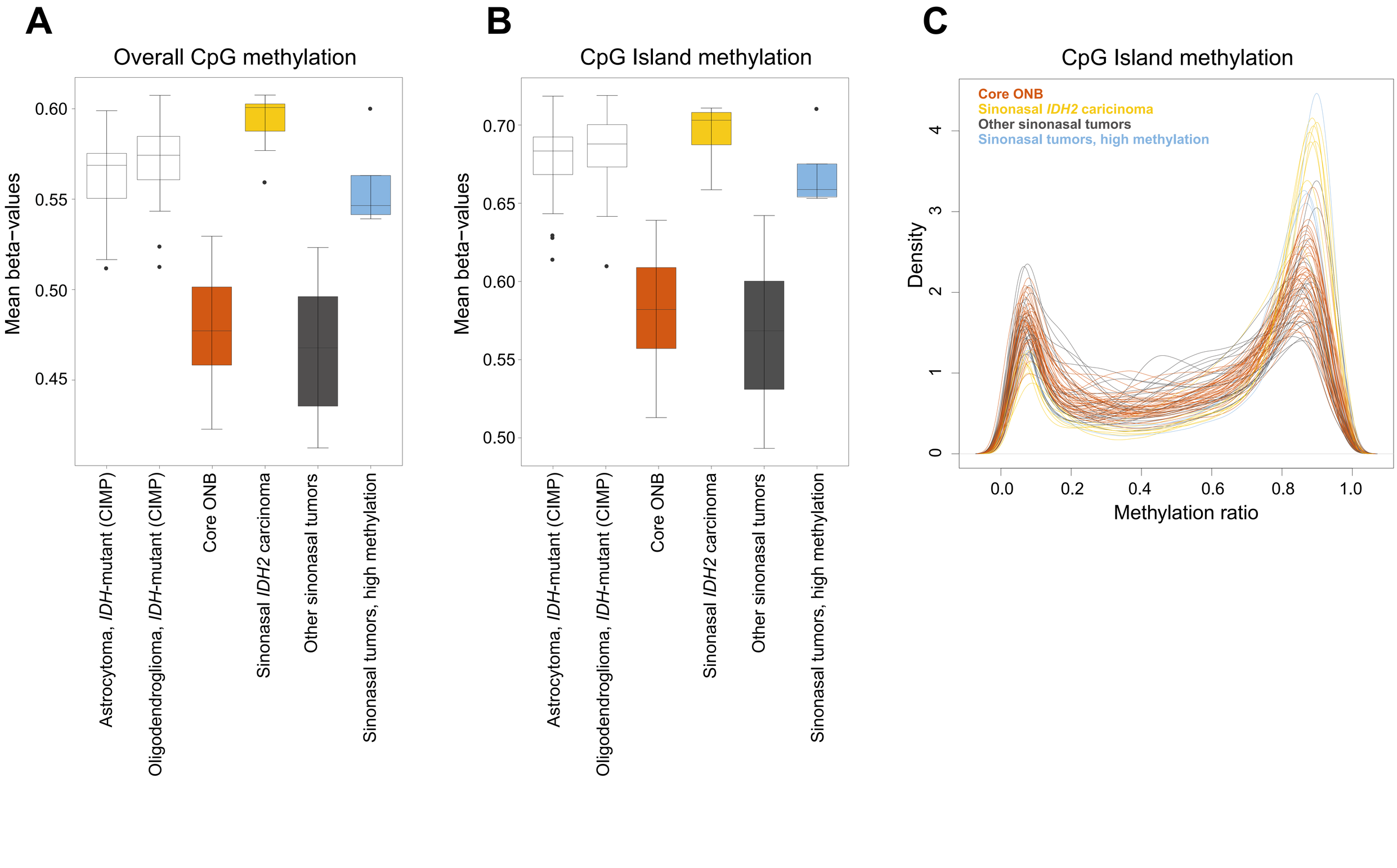

Supplementary Figure 4

A

	Core ONB n=42	Sinonasal tumors, high meth. n=4	Sinonasal *IDH2* carcinoma n=8	
Median age	62 y	28.5 y	52.5 y	p=0.007 *
Gender				
male	50%	50%	87.5%	
female	50%	50%	12.5%	p=0.1436

* Median age: core ONB vs. Sinonasal tumors, high meth. are significantly different

B